

Review

From intrusion-related to orogenic mineralization: The Wasamac deposit, Abitibi Greenstone Belt, Canada

Nicolas Mériaud ^{a,*}, Michel Jébrak ^b^a Centre for Exploration Targeting, School of Earth Sciences, University of Western Australia, Crawley, Western Australia 6009, Australia^b Département des Sciences de la Terre et de l'Atmosphère, Université du Québec à Montréal (UQAM), C.P. 8888 Succ. Centre-ville, Montréal, Québec H3C 3P8, Canada

ARTICLE INFO

Article history:

Received 20 April 2016

Received in revised form 19 January 2017

Accepted 20 January 2017

Available online 24 January 2017

Keywords:

Orogenic gold

Intrusion-related

Alkaline alteration

Gold telluride

ABSTRACT

The Wasamac deposit is an example of Archean greenstone-hosted gold deposit located in the Abitibi Belt, 15 km southwest of Rouyn-Noranda. The deposit is hosted by a second-order ductile shear zone of the Cadillac–Larder Lake Fault Zone (CLLFZ), known as the Francoeur–Wasa Shear Zone (FWSZ). It regionally sits at the boundary between the orogenic gold district of Noranda and the Kirkland Lake gold district dominated by intrusion-related gold systems. This specific location in-between two different gold mineralization environments sets the Wasamac deposit apart as a prime candidate for investigating hydrothermal processes along the CLLFZ. Within the Wasamac deposit, gold distribution is constrained to the altered mylonitized portion of the FWSZ; lode systems are absent. Hydrothermal alteration and associated disseminated mineralization occurs as a replacement of the Blake River Group metavolcanic units. The hydrothermal signature displays two distinct alkaline alteration assemblages: potassic and albitic, each associated with specific gold characteristics. (1) Potassic alteration is characterized by the crystallization of microcline, carbonates and quartz. Within this assemblage gold is associated with porous pyrite enriched in Te–Ag–Au–Mo–Pb–Bi–W, deposited under oxidizing conditions. Such characteristics are widely described in the Kirkland Lake area, and are found in examples of syenite-related mineralization, such as the Beattie and Malartic gold deposits. (2) The albitic alteration assemblage, composed of albite, sericite and carbonates, reflects more reduced hydrothermal conditions with mineralization characterized by free native gold. This hydrothermal event is coeval with the brecciation of early gold-rich pyrite reflecting a structural overprint that controlled late-stage gold characteristics. These alteration and structural features are common in orogenic gold deposits both worldwide and regionally, particularly at the neighbouring Kerr–Addison and Francoeur deposits, and in lode-gold systems such as in the Sigma–Lamaque deposit.

The gold mineralization at Wasamac has similar characteristics to both intrusion-related gold systems and structurally controlled orogenic gold deposits. Hydrothermal and structural crosscutting relationships at Wasamac indicate that a structurally controlled hydrothermal event overprinted earlier potassic magmatic-hydrothermal alteration. This observation supports a multistage process of gold concentration during which new gold characteristics, metal anomalies, fluid conditions and alteration assemblages replaced earlier stages of gold enrichment, in places completely obliterating previous signatures. We propose that the Wasamac deposit was originally related to an alkaline intrusion buried at depth beneath the Francoeur–Wasa Shear Zone.

© 2017 Elsevier B.V. All rights reserved.

Contents

1. Introduction	290
2. Regional geological setting	291
3. Geological setting of the Wasamac deposit	291
3.1. Lithology and stratigraphy	291
3.2. Structural characters	293

* Corresponding author.

E-mail address: meriaud.nicolas@gmail.com (N. Mériaud).

3.3.	Hydrothermal alteration	295
3.4.	Gold mineralization	297
4.	Geochemistry of alteration	297
5.	LA-ICP-MS characterization of pyrite zonation	299
6.	Discussion	302
6.1.	The Wasamac deposit: An early hydrothermal gold enrichment with a magmatic affinity	302
6.1.1.	K-feldspar hydrothermal alteration signatures	302
6.1.2.	Early gold mineralization	303
6.2.	The Wasamac deposit: Structural and hydrothermal overprint and gold remobilization	303
6.2.1.	Albitic hydrothermal alteration signature	303
6.2.2.	From trapped invisible tellurides to free native gold	303
6.3.	Genesis of the Wasamac deposit	305
7.	Conclusions	306
	Acknowledgements	306
	Appendix A	306
	Sampling and analytical methods	306
	References	306

1. Introduction

Throughout the last few decades, numerous studies have characterized the conditions of gold transport and deposition, the tectonic settings and the timing of epigenetic lode-gold mineralization in greenstone belts (Colvine et al., 1988; Sibson et al., 1988; Robert, 1990; McCuaig and Kerrich, 1998; Goldfarb et al., 2001, 2005; Groves et al., 1998, 2003; Groves and Santosh, 2015; and references therein). As the world's second-most important gold producer after paleoplacers, Precambrian greenstone belts host three types of deposits: orogenic, intrusion-related and volcanogenic (Poulsen et al., 2000; Dube and Gosselin, 2007). Archean orogenic and intrusion-related gold deposits along major crustal structures share the following characteristics: (1) post-peak metamorphic hydrothermal timing; (2) thermal equilibrium with the wallrocks during their formation; (3) H₂O-CO₂ ore-forming fluids of low to moderate salinity; (4) hydrothermal gains of K, S, Si and Au with variable additions of As, B, Bi, Na, Sb, Te and W, and low base-metal contents; and (5) depths of formation ranging from 3 to 20 km in the crust (Colvine et al., 1988; Groves et al., 1998; Goldfarb et al., 2001). However, since the late 1990s, several authors have proposed that “intrusion-related gold system” be treated as a separate group from orogenic deposits, along the lines of the porphyry copper classification long advocated by Sillitoe (1979, 1991, 2002). Within Archean terranes, intrusion-related deposits differ from other gold deposits in the following ways: (1) they present a spatial association with intrusions of intermediate to felsic compositions that lie near the boundary between ilmenite and magnetite series; (2) the involvement of carbonic hydrothermal fluids; (3) a metal assemblage that combines gold with elevated concentrations of one or more of Bi, W, As, Mo, Te or Sb, accompanied by low concentrations of base metals; (4) a post-collisional timing during transitional tectonic regimes; and (5) a specific tectonic setting close to lithospheric boundaries and above previously metasomatized subcontinental lithospheric mantle (Thompson et al., 1999; Lang and Baker, 2001; Robert, 2001; Hart and Goldfarb, 2005; Mair et al., 2011). These criteria may vary within this group, such as the petrographic characteristics or the oxidation state of the intrusions themselves. Accordingly, subgroups such as subalkaline, metaluminous, I-type, reduced and oxidized intrusions were proposed based on magma sources, the processes involved and contamination by assimilation (Thompson et al., 1999; Lang et al., 2000; Robert, 2001; Hart et al., 2004; Hart, 2005).

Aside from controversies on terminologies mostly relating to overlapping characteristics with classic orogenic deposits (Hart, 2005; Phillips and Powell, 2015), a lively debate concerns the

source of fluids and metals for gold mineralization in greenstone belts (Goldfarb and Groves, 2015). Since the early 1980s, two models have been proposed in Archean terranes: (1) Metamorphic fluids for orogenic gold mineralization (Kerrich, 1983; Perrault et al., 1984; Cox et al., 1991; Groves et al., 1998; Beaudoin and Pitre, 2005; Zhang et al., 2014) and (2) Magmatic-hydrothermal fluids for intrusion-related mineralization (Hodgson, 1985; Thompson et al., 1999; Lang and Baker, 2001; Mair et al., 2011; Helt et al., 2014; Bigot and Jébrak, 2015). In addition, establishing a temporal link between magma and gold mineralization in complex and evolving metamorphic belts remains equivocal (Goldfarb and Groves, 2015).

In the Abitibi Greenstone Belt, quartz-carbonate (+/- tourmaline) vein systems hosted in shear zones occur along major structural corridors, such as the Cadillac-Larder Lake and Destor-Porcupine fault zones. They represent 81% of the total Canadian gold production, and belong to the class of orogenic gold mineralization (Robert, 1990; Poulsen et al., 2000; Dube and Gosselin, 2007). Robert (2001) introduced the intrusion-related gold group of deposits as a distinct class of mineralization in the Abitibi Belt. Spatially, both metallogenic environments are distributed along the Cadillac Larder-Lake Fault Zone (CLLFZ) and lower-order related structures. To the east, the Val-d'Or district hosts typical examples of orogenic gold deposits, such as the Sigma and Lamaque mines (Robert and Brown, 1986a,b). Bordering this district to the west, the Malartic district hosts a bulk-tonnage intrusion-related gold deposit (Helt et al., 2014; De Souza et al., 2015; Gao et al., 2015). However, both styles of gold mineralization overlap in some places (Fig. 1). In the western portion of the CLLFZ, most gold deposits of the Kirkland Lake and Matachewan areas are spatially linked with syenitic intrusions and display highly oxidized alkaline alteration assemblages (Robert, 2001; Zhang et al., 2014; Rafini, 2014). In the Rouyn-Noranda area, the CLLFZ shows disseminated gold mineralization associated with brittle-ductile faults and lodes displaying ultramafic- to alkaline-derived alteration footprints (Couture and Pilote, 1993; Legault and Rabeau, 2007; Rafini, 2014). Between these two districts, 15 gold deposits and showings hosting a total of roughly 200 metric tons of gold display both intrusion-related and orogenic mineralization (Smith et al., 1993; Legault and Rabeau, 2007; Rafini, 2014).

Located between Rouyn-Noranda and Kirkland Lake gold districts and sitting along the second-order Francoeur-Wasa Shear Zone (FWSZ), the Wasamac deposit (83.46 t Au) shares similarities with both intrusion-related and orogenic gold deposits. Robert (2001) highlighted strong similarities between deposits of the Kirkland Lake district and the Francoeur deposit near Wasamac. The intriguing continuity between these two differently classified

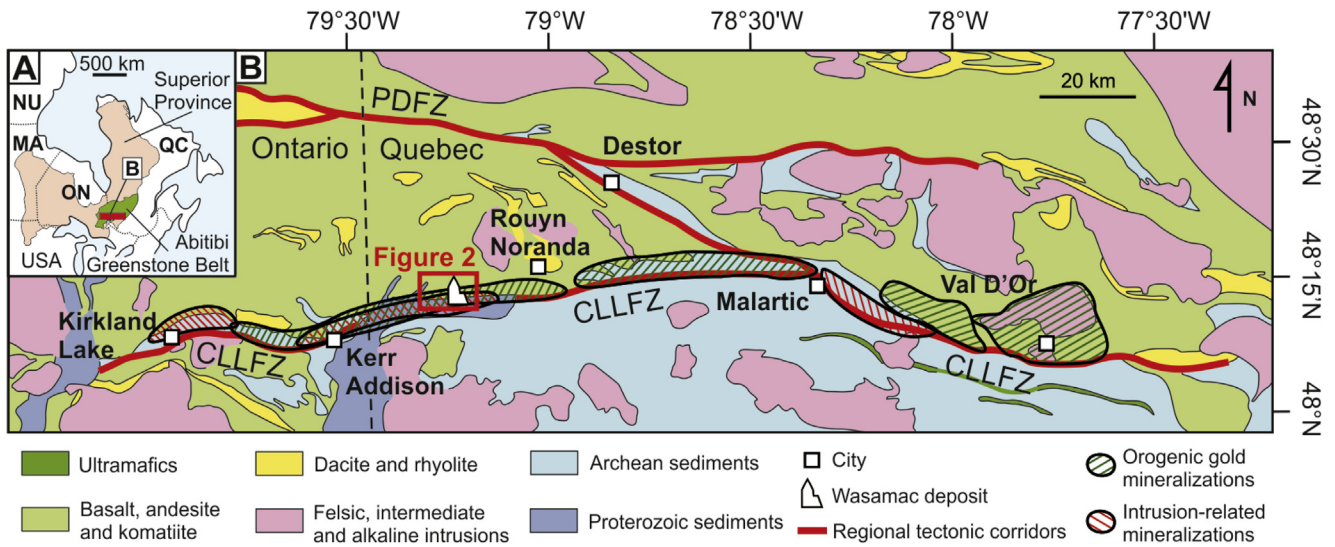


Fig. 1. The main structural corridors of southern Abitibi: the Cadillac Larder Lake Fault Zone (CLLFZ) and the Porcupine Destor Fault Zone (PDFZ). Disposition of orogenic and intrusion-related styles of mineralization with respect to the hydrothermal fields proposed by Rafini (2014). Modified from Robert (2001); Rabreau et al. (2013) and Rafini (2014).

deposits led Robert (2001) to suggest a re-examination of the classification of some gold deposits along the CLLFZ. Our work focuses on the geochemical and mineralogical descriptions of the alkaline alteration and mineralization at the Wasamac deposit, bringing to light new data on this transitional metallogenic region.

2. Regional geological setting

The Abitibi Subprovince is located in the southeastern part of the Superior Province. It represents the largest greenstone belt of the Canadian Shield with an extension of 700 km by 300 km. Its early volcano-plutonic construction has been dated from ca. 2750 to 2690 Ma (Corfu, 1993; Ayer et al., 2002). The southern Abitibi Belt is notably composed of the metavolcanic units of the Blake River, Piché and Malartic groups, which range in composition from ultramafic to felsic and display tholeiitic to calc-alkaline affinities (Goodwin, 1982; Corfu, 1993; Daigneault et al., 2002; McNicoll et al., 2014). Several structural models have been proposed for the Southern Abitibi Belt, involving up to eight distinct events (Daigneault et al., 2004; Ayer et al., 2005), which could be summarized as follows. Deformation (D1) is locally described as east-west trending folds and local thrusting related to a N-S horizontal shortening event between ca. 2687 and ca. 2680 Ma (Robert, 2001). It has been proposed that this episode is coeval with the emplacement of late tonalite-trondjhemite intrusions mostly described in Ontario and dated at ca. 2685 Ma, with no extrusive equivalents (Corfu et al., 1991; Sutcliffe et al., 1993; Robert, 2001). A subsequent uplift and erosion event deposited Timiskaming-type fluvial-alluvial sedimentary units between ca. 2676 and ca. 2670 Ma (Ayer et al., 2005). This sedimentation is coeval with the emplacement of early, dominantly alkaline, syn-tectonic plutons (Corfu et al., 1991; Robert, 2001). It closely predates the north-over-south thrusting movement (D2), then followed by the succession of dextral transpressive accommodation and local renewed thrusting (D3) from ca. 2673 Ma to ca. 2660 Ma (Robert, 2001; Daigneault et al., 2004). The formation of the CLLFZ is attributed to these two tectonic events (Robert, 2001; Daigneault et al., 2004). An exhumation event is recognized at ca. 2660 Ma near the Malartic segment, manifested as local extensional movements along major structural corridors, such as the kinematics observed in the Granada deposit (Daigneault et al., 2004). Late shearing

occurrences extended the tectonic activity of the CLLFZ to around ca. 2643 Ma at the Lamotte Pluton (Daigneault et al., 2004).

The structural evolution of the Abitibi Greenstone Belt is still the subject of controversies, particularly the debate about the driving processes involved in Archean early crustal construction and deformation. Plate-tectonic models propose that a horizontal oblique-plate convergence during a 60 Ma polyphased tectonic history were responsible for Abitibian crustal architecture (Daigneault et al., 2004). Alternative models suggest that mantle dynamics and/or gravity driven processes controlled the formation and deformation of Archean terranes (Bédard et al., 2013; Thébaud and Rey, 2013; Harris and Bédard, 2014). Metamorphic assemblages range from sub-greenschist to sub-amphibolite grade and were dated in southern Abitibi from ca. 2677 to ca. 2643 Ma (Jolly, 1978; Powell et al., 1995; Dube and Gosselin, 2007).

Sampling and analytical methods undertaken for this study are provided in the appendix section of the paper.

3. Geological setting of the Wasamac deposit

3.1. Lithology and stratigraphy

The Wasamac deposit is located along the Francoeur-Wasamac Shear Zone (FWSZ), a second-order fault parallel to and 2.5 km north of the CLLFZ. The FWSZ traverses the meta-volcanic units of the Blake River Group (Fig. 2A). Along this break, which also hosts the Francoeur deposit (Couture and Pilote, 1993), units of the Blake River Group were tilted toward the north and follow the same east-west trend. Near the Wasamac deposit, the Blake River metavolcanic units are composed of three lithologies, all intermediate to felsic in composition (Pilote and Couture, 1989; Couture and Pilote, 1993).

Massive andesite is the most common lithology and is the principal host of the FWSZ from surface to depth (Fig. 2B). It locally displays a variety of volcanic textures including aphanitic, porphyritic, amygdaloidal, pillowed and brecciated. The thickness of andesitic volcanic breccia layers locally exceeds 100 m. Clasts are composed of andesite-rhyodacite and intermediate to felsic tuff blocks in a massive or lapilli-crystal tuff matrix. These synvolcanic fragments are commonly centimeter-scale and may locally reach several decimeters (Fig. 3A). They generally represent less than

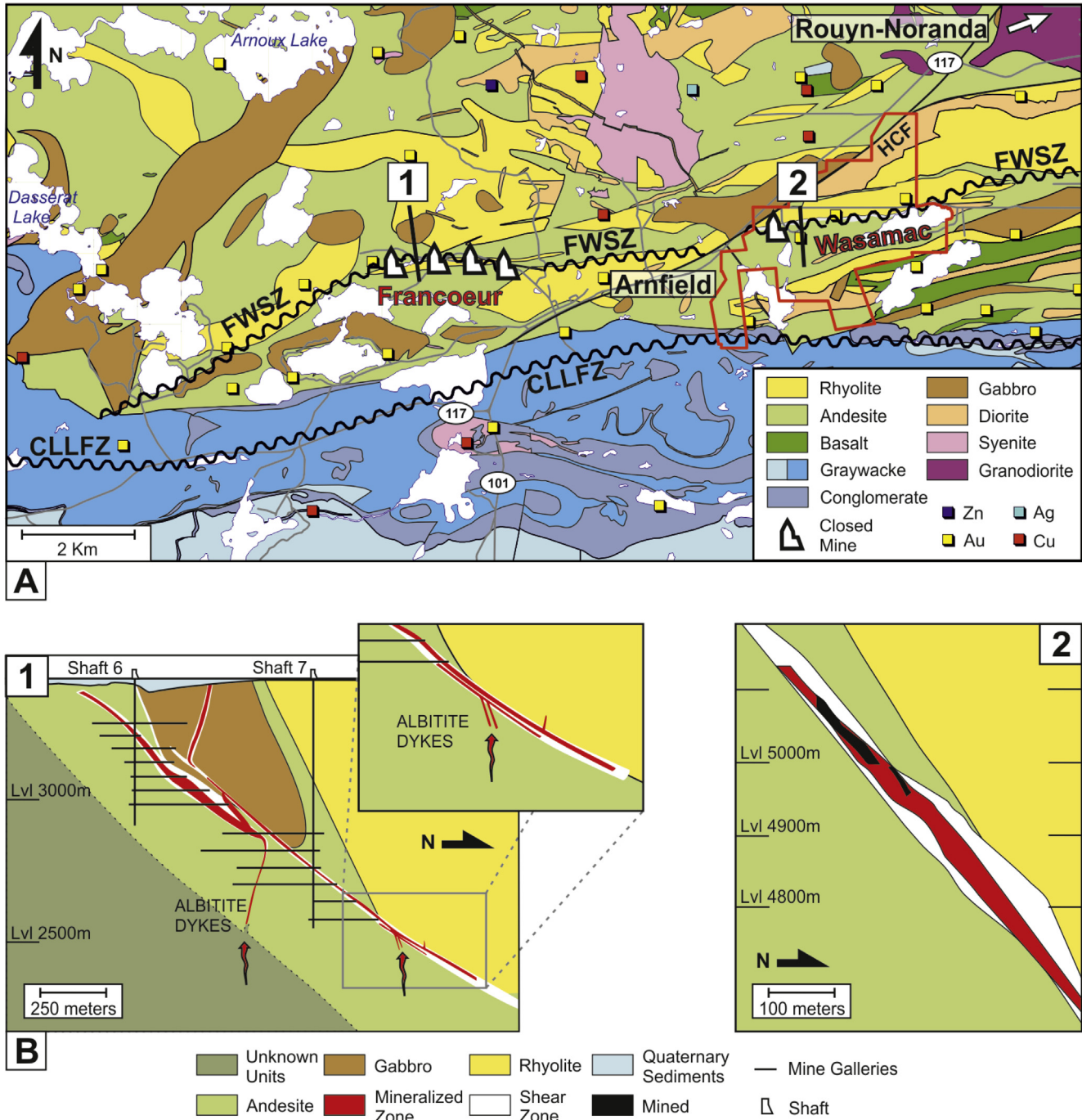


Fig. 2. (A) Geological map of the Francoeur-Wasa Shear Zone (FWSZ). 1 and 2 lines refer to Fig. 2B cross-sections of Francoeur and Wasamac deposits. (B) Simplified typical geological cross-sections of Francoeur (1) and Wasamac (2) deposits. Both deposits are situated within the FWSZ and display similar geologic environments. Albitite dykes connected to the shear zone are described in Francoeur but none are observed in Wasamac.

30% of the rock. Clasts frequently show an angular shape and locally present a coronitic texture. These petrographic characteristics are indicators of polyphase pyroclastic volcanic activity from at least one proximal volcanic source.

Rhyolitic units are mostly aphanitic, locally porphyritic with millimeter-scale quartz and feldspar phenocrysts. A few volcanogenic textures were identified in places, such as flow banding and breccia. The rhyolitic units range from greyish to pinkish beige reflecting local pervasive albitic and sericitic alteration spatially associated with micron-scale fractures that increase in abundance towards the shear zone. Rhyolite is located in the hanging wall of

the FWSZ (Fig. 2B) and shows brittle deformation instead of the ductile deformation exhibited by the andesitic units.

Two generations of intrusive units were observed to cut across the metavolcanic units of the Wasamac deposit in drill core: gabbro and syenite, both of which are locally deformed by the FWSZ. The gabbros are of calc-alkaline affinity and occur either as coarse-grained stocks with fine-grained contacts or as meter-scale aphanitic to fine-grained dykes and sills. The grey syenite dykes are generally meter-scale, rarely reaching a decameter or more in thickness. Their contact with the host rock is sharp and straight. In places, and typically close to the FWSZ, contacts may

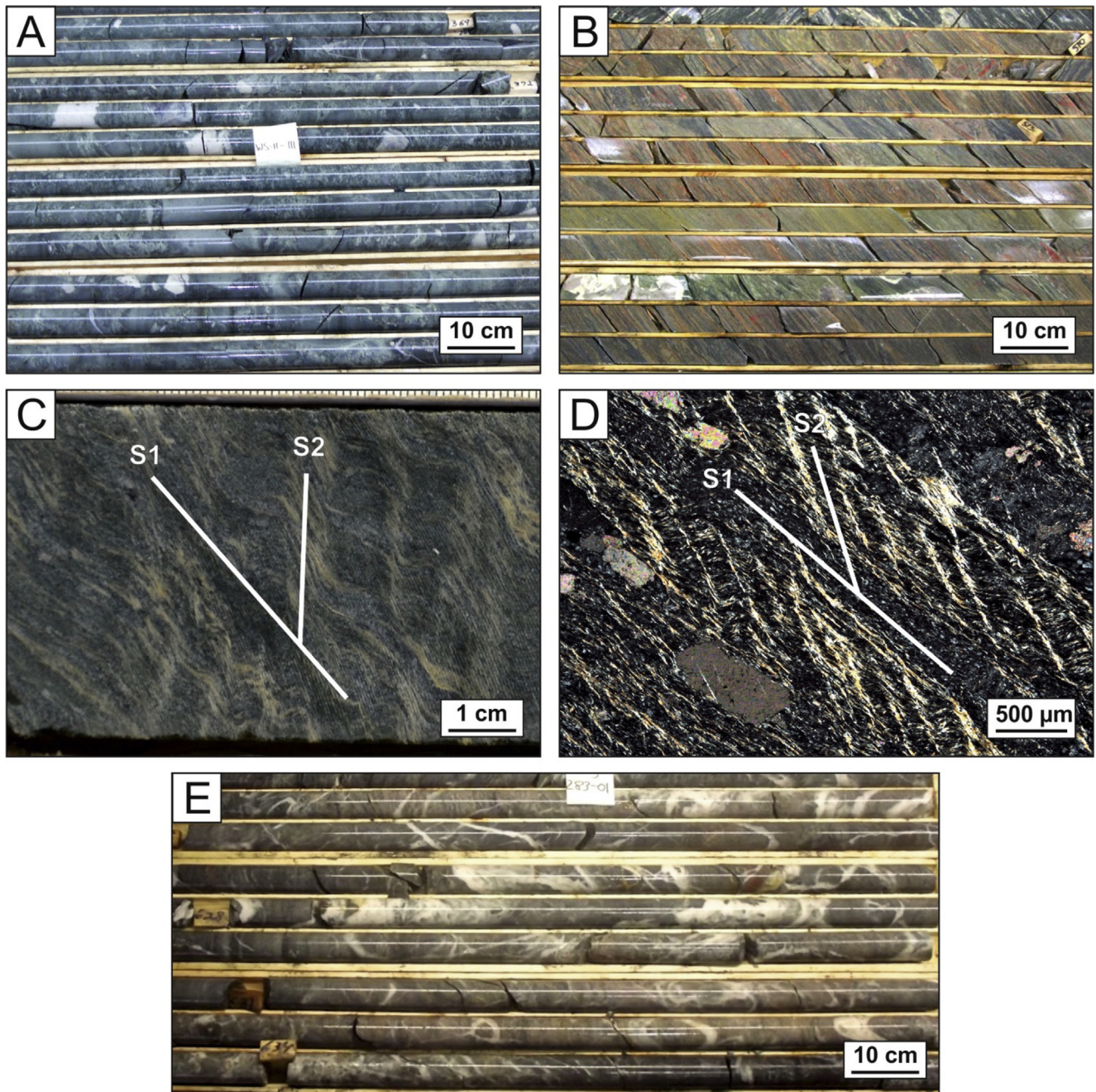


Fig. 3. (A) Clastic tuff with centimetric rhyodacite, rhyolite and lapilli tuff blocs in an intermediate lapilli-tuff matrix. (B) Typical alteration of the FWSZ mylonite of Main Zone and Zone 3. The shear zone displays a diversity of alteration colorations related to several hydrothermal footprints. The most common alteration spatially associated with the mineralization is the albite-pyrite-sericite-carbonate assemblage. The red-coloured potassic alteration is also identified. (C) Main schistosity (S1) and crenulation cleavage (S2) showing centimetric asymmetric Z-shaped folds affecting a moderate altered andesite. (D) Main schistosity (S1) and crenulation cleavage (S2) in thin section. (E) Intersection between the Wasamac Shear Zone and the Horne-Creek Fault. Quartz veins and veinlets from the Horne-Creek Fault crosscut the brownish alteration of the FWSZ.

exhibit brecciation with a red-purple tint caused by pervasive potassic alteration with rare disseminated pyrite and very low gold values (below 25 ppb). The syenite dykes cut across the gabbro and are thus the last intrusive event identified near the Wasamac deposit.

3.2. Structural characters

Along the Wasamac deposit, the second-order FWSZ is an east-trending ($\sim 260^\circ$) mylonitic structure dipping 55° to the north. It represents a thick, intense ductile shear zone affecting volcanic

units, associated with strong hydrothermal alteration (Couture and Pilote, 1993) (Fig. 3B). The FWSZ occurs close to the contact between andesite and rhyolite, and is mostly hosted in andesite. Both contacts of the FWSZ are gradual over a few meters. They are marked by an increasing concentration of barren carbonate veinlets that become progressively sheared towards the deformation zone. The thickness of the shear zone varies from several meters to over a hundred meters, and generally widens with depth. Richmond Mines Inc. defined four economic zones broadly distinguished by variations in shear zone thickness; they are, from west to the east, the Main Zone and zones 1, 2 and 3.

Host lithologies display two kinds of responses to deformation. Andesite and gabbro exhibit weak to intense ductile deformation, whereas silica-rich units (e.g., rhyolite and potassic-altered units) are frequently brecciated within low deformation zones. The latter are present as centimeter- to meter-scale elongated slivers of less deformed brecciated units within the FWSZ. This rheological contrast may be the result of structural partitioning in which competent K-altered silica-rich rocks are not mylonitized compared to the surrounding albitized and chlorite-rich less competent units.

Brecciation may also be observed beyond the shear zone, most commonly at the contacts between felsic and alkaline units.

The FWSZ is characterized by strong mineral stretching of altered and unaltered mineral assemblages attributed to S1 foliation. This well-developed S1 fabric obliterated primary volcanic textures and shows as mylonitic schist (Fig. 3B). According to kinematic indicators (e.g., C-type shear bands, asymmetric pressure shadows), S1 foliation reflects reverse movement with dextral components. A second foliation, S2, is also recognized within the

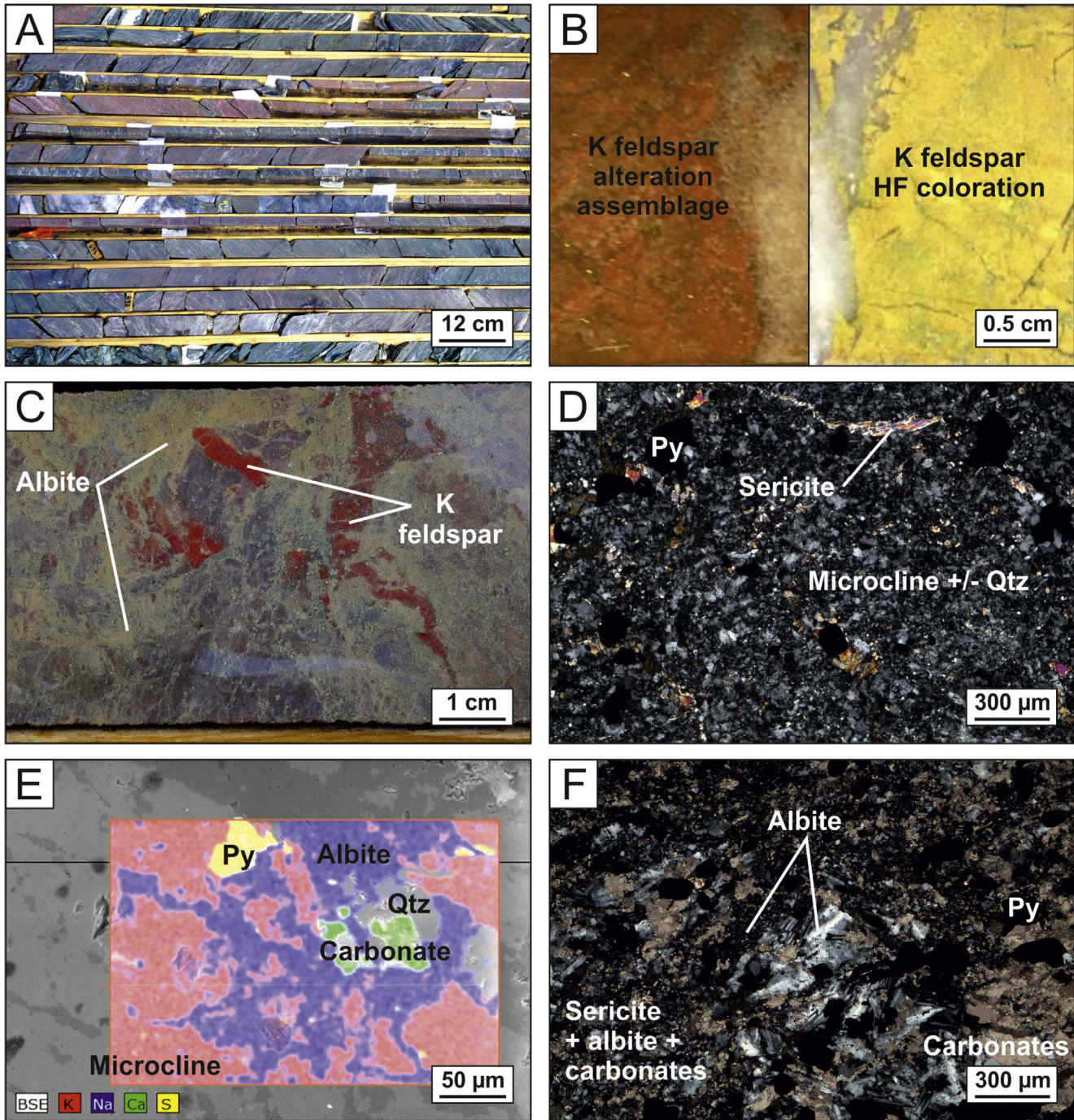


Fig. 4. (A) Typical alteration of the FWSZ Zones 1 and 2. Alteration is here restricted to intense red coloured fractured units with sharp contacts, composed of micron-scale K-feldspars, sericite, carbonate and pyrite. (B) Photograph of the typical K-feldspar brick-red coloration (left) and cobaltinitrite coloration of the same sample (right). (C) Contact between the two alteration facies: pervasive albitization crosscuts potassic-altered brecciated veinlets. (D) Photograph of transmitted polarised light microscopy of potassic alteration facies. Composition is micron-scale hematized microcline, sericite, pyrite and carbonate. (E) SEM coloration of albitic and potassic alterations. The microphotograph displays a brecciated potassic-altered unit filled with the albitic hydrothermal assemblage as a matrix, supporting that albitization crosscuts the potassic alteration. (F) Photograph of transmitted polarised light microscopy of albitic alteration facies, composed of micron-scale albite, sericite, carbonate and pyrite.

FWSZ as locally developed “shear band” crenulation cleavage, which was observed forming asymmetric Z-type subvertical folds (Fig. 3C and D). S2 never becomes penetrative and remains a weak structural footprint. Similar S2 crenulation cleavage has been identified regionally along the CLLFZ and second-order fault zones, where it indicates dextral transcurrent motion (Daigneault et al., 2004; Ispolatov et al., 2008; Zhang et al., 2014). At Wasamac, S2 is thus related to the last regional ductile tectonic footprint cited by these authors. The minerals in both the potassic and albitic alteration assemblages are affected by S1 and S2, implying that the hydrothermal activity is pre- to syn-tectonic.

The regional Horne-Creek Fault (HCF) was also intersected by drilling at the Wasamac deposit. The HCF is identified by a 4 to 25 meters wide network of quartz veins and stockworks, associated with an intense silicification of the host rock. One-meter gouge contacts were also systematically observed along both sides of the fault. Regionally, the movement of the HCF has been interpreted as sinistral where it offsets the FWSZ (Fig. 2A). The cross-cutting relationship between the two faults demonstrates that quartz stockworks from the HCF postdate the FWSZ (Fig. 3E). No shearing was observed in HCF intervals in drill core, and this fault is thus assumed to record a late brittle deformation event.

3.3. Hydrothermal alteration

Hydrothermal alteration is restricted to the mylonitized portion of the FWSZ. Gold mineralization is strictly related to potassic and albitic pervasive alteration assemblages in which gold is spatially associated with disseminated pyrite. Potassic metasomatism is associated with a well-developed Microcline-rich assemblage, whereas sodic metasomatism is recognized by an albite-dominated assemblage. These alteration signatures display short transition zones with fresh rocks.

Potassic alteration is observed as a red brick-colored aphanitic assemblage (Fig. 4A–C). It is mostly composed of microcline, quartz and pyrite with smaller amounts of sericite and carbonates (Fig. 4D). Biotite was not present in the samples examined. The intense color is due to inclusions of dusty hematite trapped in

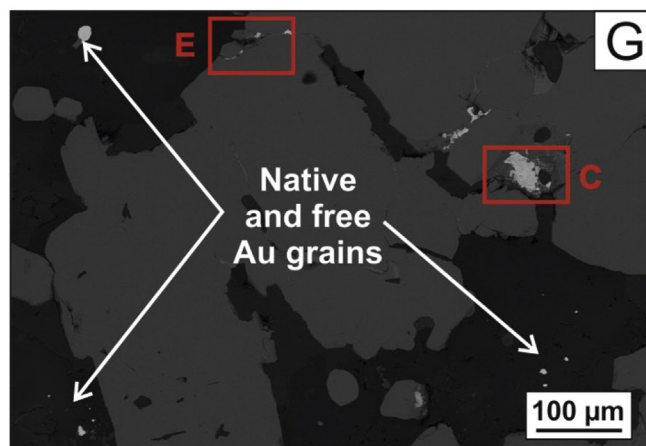
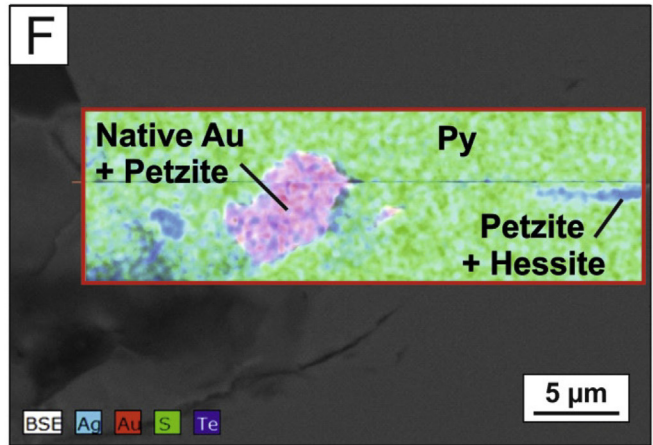
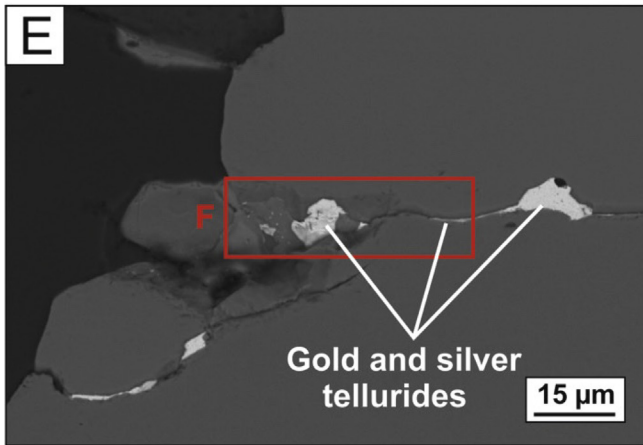
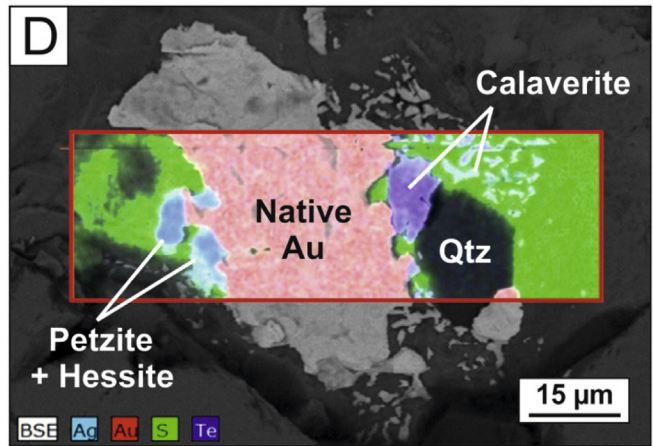
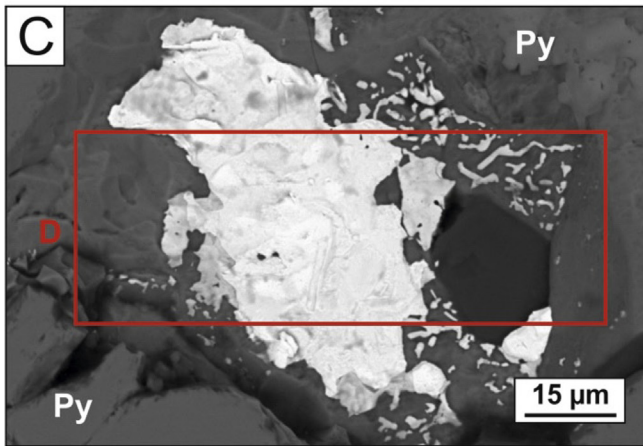
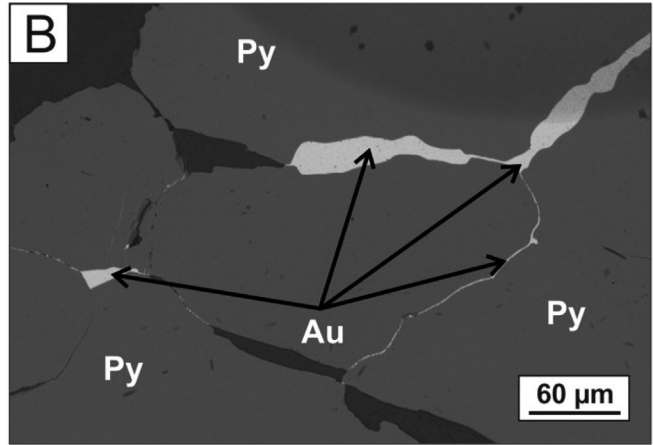
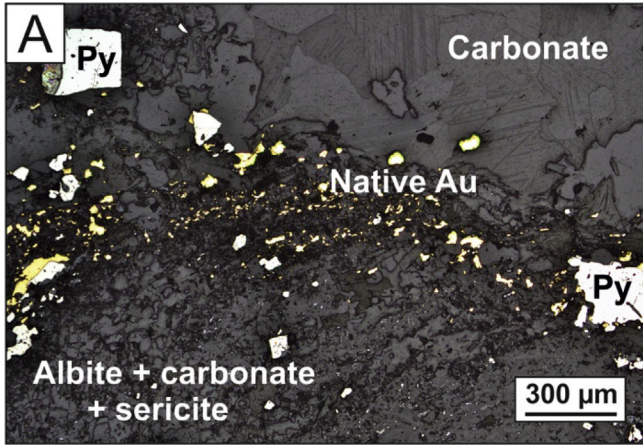
the microcline structure. This alteration usually presents sharp contacts with its host rocks and frequently appears as dyke-like units (Fig. 4A). Fracturing and clast-supported brecciation is also commonly observed affecting potassic-altered units (Fig. 4C and E), particularly at the contacts with the host rock. The matrix is composed mostly of albite, carbonate, sericite, chlorite, quartz and pyrite with rare visible gold grains (Fig. 4E and F). Clasts vary in size from millimeters to decimeters, and feature angular and subrounded shapes roughly oriented along S1. A localized cataclastic fabric is observed along the direction of main FWSZ schistosity, displaying millimeter- to centimeter-scale potassic-altered clasts in an albite-dominated matrix. Late quartz veinlets may also be observed carrying rare chalcopyrite and remobilized native gold. Similar oxidized potassic alteration was observed in fractured portions of syenite dykes away from the shear zone. These altered dykes display limited gold enrichment of up to 25 ppb compared to least-altered syenite dykes containing an average of 5 ppb Au. A similarly altered undeformed pyrite-rich syenite dyke adjacent to the Francoeur orebody yielded 100 ppb Au, far above host rock background levels.

Albitization is described within the Wasamac deposit as a fine-grained beige-colored assemblage with greyish to purplish hues. It occurs as pervasive alteration affecting metavolcanic units. It is composed of micron-size grains of albite, quartz, carbonates, pyrite and sericite (Fig. 4F). Sulfur content is higher than in the potassic facies, commonly reaching 5% and locally 20%. Albitization affects unaltered volcanic units and overprints potassic alteration.

Potassic and albitic alteration assemblages indicate a significant change in the oxidation state of the hydrothermal fluids. The abundant hematite causing the intense red color of the potassic assemblage and its low pyrite content reflects highly oxidized hydrothermal activity (Cameron and Hattori, 1987; Thompson et al., 1999). Besides, the pyrite-rich albitic assemblage with fewer oxide minerals records a more reducing hydrothermal environment. The cross-cutting relationship between the two facies is observed in brecciated zones where clasts of potassic-altered rock are cut by fractures filled with a pyrite-enriched albite assemblage, or are surrounded by this albitic assemblage in matrix-supported

	Main Zone	Zone 1	Zone 2	Zone 3
Overall gold mineralogy (%)	80 60 40 20 Native gold Gold tellurides			
Pyrite and gold mineralogical relationship	Free gold : 51.8% Average grain size : 8.7µm Gold attached to Py : 14.2% Average grain size : 4µm Gold locked into Py : 33.5% Average grain size : 2.6µm	Free gold : 32.9% Average grain size : 10.6µm Gold attached to Py : 16.8% Average grain size : 2.9µm Gold locked into Py : 50.3% Average grain size : 2.1µm	Free gold : 26.5% Average grain size : 11.1µm Gold attached to Py : 25.8% Average grain size : 2.7µm Gold locked into Py : 47.6% Average grain size : 2.1µm	Free gold : 47.5% Average grain size : 12.6µm Gold attached to Py : 8.8% Average grain size : 3.9µm Gold locked into Py : 43.8% Average grain size : 2.8µm
Telluride minerals related to the mineralization	Petzzite (Ag ₃ AuTe ₂) Calaverite (AuTe ₂) Melonite (NiTe ₂) Altaite (PbTe) Tellurium (Te)	Petzzite (Ag ₃ AuTe ₂) Hessite (Ag ₂ Te) Altaite (PbTe)	Petzzite (Ag ₃ AuTe ₂) Calaverite (AuTe ₂) Muthmannite ((Au,Ag) ₂ Te ₄) Sylvanite ((Ag,Au) ₂ Te ₄) Hessite (Ag ₂ Te) Altaite (PbTe) Tellurobismuthite (Bi ₂ Te ₃) Melonite (NiTe ₂)	Petzzite (Ag ₃ AuTe ₂) Calaverite (AuTe ₂) Hessite (Ag ₂ Te)

Fig. 5. Mineralogy of gold from metallurgical tests within Wasamac deposit's four economic zones along the longitudinal axis of the shear zone. Zones 1 and 2 mostly display telluride-gold minerals (calaverite and petzzite) whereas Main Zone and Zone 3 display native gold. Both the spatial relationships between gold and pyrite and the gold grain size associated also support the longitudinal zonation of mineralization footprints typical of each alteration facies. Data collected from over 1200 gold grains by SGS.



facies. The albitic assemblage progressively replaces the potassic assemblage. The clear crosscutting relationship and contrasting redox conditions indicates two hydrothermal events.

3.4. Gold mineralization

Ore zones are restricted to the altered mylonitic portion of the FWSZ. Gold occurs as small telluride minerals and as native grains. Arsenic-free pyrite is the only sulfide present in the two alteration assemblages previously described, except for rare and sporadically disseminated chalcopyrite grains.

In the albitic alteration assemblage documented in the Main Zone and Zone 3, more than 98% of gold occurs in the native state, principally as disseminated free grains (Fig. 5). The average size of free gold grains is 5.7 μm, and some exceed 10 μm. According to SEM results, native gold contains an average of 8% silver. Gold is spatially associated with pyrite-rich zones where the sulfide content frequently exceeds 5%. Pyrite displays a nonporous texture and rarely contains inclusions of gold. It is locally affected by brecciation characterized by micron-scale cataclasis zones in a cement of carbonates, albite, sericite, quartz and chlorite, within which native gold occurs as free grains or as fracture fillings in pyrite (Fig. 6A and B).

In the dominant potassic alteration of Zones 1 and 2, 50% of the gold occurs as the tellurides petzite (Ag₃AuTe) and calaverite (AuTe₂). Over 80% of telluride minerals are observed along the contacts of pyrite grains that are <100 μm in size and <5% in abundance. Gold tellurides occur as very fine grains, averaging 3.5 μm across; other tellurides (Ag, Bi, Pb and Ni) are present in trace amounts. Gold tellurides mostly occur as inclusions in pyrite and fillings related to localized pyrite porosity. More rarely, they occur as free grains disseminated in the alteration assemblage, or occasionally trapped in microcline, titanite, hematite or sericite. Gold tellurides also frequently fill pyrite fracture planes less than 5 μm wide (Fig. 6C–G), whereas native gold is found in wider fractures (>5 μm). This relationship between pyrite fracture size and gold mineralogy is a characteristic of Wasamac mineralization. The erratic distribution of pyrite fractures of all sizes suggest they formed as part of a single late brittle event. This is supported by the observation of contacts between the two gold-bearing phases in the same fracture in which gold tellurides occupy the narrower deeper part and native gold the wider outer part.

Gold mineralogy, average grain size and spatial association with As-free pyrite are specific for each alteration assemblage. Hence, similar to the alteration assemblages, gold follows the same zonation pattern at the scale of the property (Fig. 5). The absence of lode systems is another specific characteristic of the mineralization at the Wasamac deposit, similar to the nearby Francoeur deposit (Couture and Pilote, 1993).

4. Geochemistry of alteration

In Archean greenstone belts, incompatible immobile elements (Zr, Y, Nb and REE) are used to define precursor lithologies and monitor the fractionation of compatible elements in tholeiitic to transitional volcanic units (MacLean and Barrett, 1993). The almost-immobility of Zr, Ti and Al during hydrothermal processes can also be used to accurately identify metamorphosed and altered

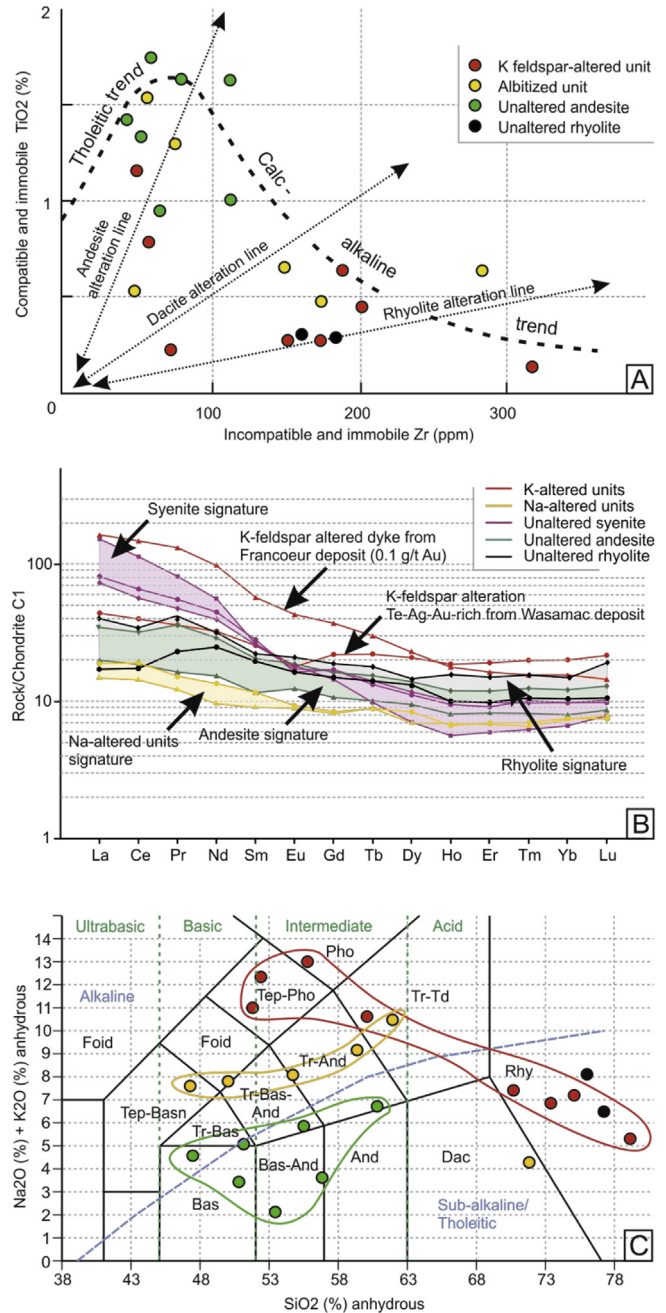


Fig. 7. (A) Diagram of immobile elements displaying altered and least-altered samples. Host rocks are andesitic and rhyolitic in composition mostly with a calc-alkaline affinity. (B) Chondrite-normalized REE diagram from unaltered and altered units. (C) Alkali and silica diagram from Lebas et al. (1986) displaying chemical patterns of altered and unaltered volcanic units in the Wasamac deposit.

volcanic precursors (MacLean and Kranidiotis, 1987), except in hyper-alkaline systems. At the Wasamac deposit, the results of this study demonstrate the immobility of Zr and Ti, and locally that of Al, Fe, Nb, Y and REE. Two sets of data can be distinguished plotting

Fig. 6. (A) Photograph of reflected light microscopy displaying free native gold associated with a cataclased zone within an albitic alteration assemblage. (B) SEM photograph of gold filling fractures in pyrite (C) SEM photograph of gold-rich fracture in pyrite. (D) SEM coloration of (C) displaying native gold and gold-silver telluride minerals filling fractures into pyrite. Thin fractures are mostly tellurium-rich, whereas wide-open fractures are native gold rich. (E) SEM image showing gold-rich fractures in pyrite. (F) Close-up of (E) showing wide-open fracture into pyrite mostly filled with native gold. Contacts with pyrite fractures show vermicular gold-silver telluride minerals. (G) Overall SEM photograph from (C) and (E) close-up photographs showing various gold mineralogy: gold-silver tellurides filling thin pyrite fracture planes, native gold filling wide fracture planes and native free gold grains.

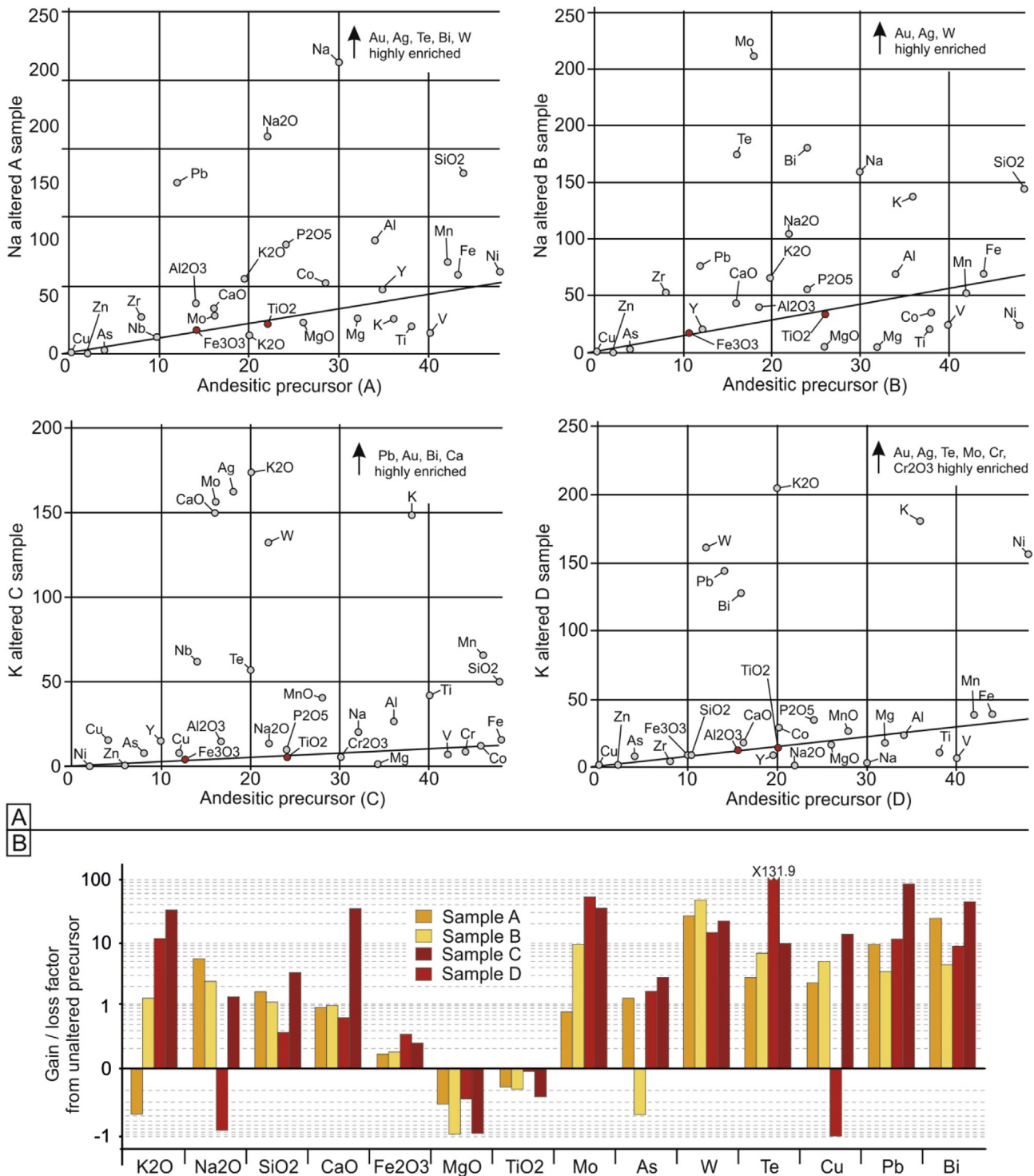


Fig. 8. (A) Isocone diagrams of selected elements in which highly altered samples are compared to their proximal unaltered host (Grant, 1986). These samples were selected from the 28 samples described in the sampling and analytical methods section. Two pairs of samples are related to albitic alteration (A and B) and two pairs are related to K-feldspar alteration (C and D). Each altered sample is enriched in elements above the immobility isochron line and is depleted in elements below the line. (B) Mass balance calculations from samples described in Fig. 8A. Calculations were produced by the Lithomoleleur software (Trépanier, 2013). An enrichment factor of 1 means a 100% gains from the unaltered protolith, mass gain for the relative element is thus twice as the original mass.

along andesite and rhyolite trends on a TiO_2 vs. Zr binary diagram, supporting that hydrothermal fluids overprint their volcanic hosts (Fig. 7A). Similar flat profiles between altered and fresh volcanic units are observed on a REE normalized-diagram (Fig. 7B). According to these results, both potassic and albitic altered units follow the geochemical characteristics of their respective volcanic hosts

supporting that alkaline alterations are the result of *in situ* hydrothermal replacement of intermediate to felsic protoliths.

Based on mobile element behaviors, the hydrothermal signatures of alteration assemblages support a strong alkali footprint, as shown in the $\text{Na}_2\text{O} + \text{K}_2\text{O}$ versus SiO_2 diagram of Lebas et al. (1986) (Fig. 7C). Fresh volcanic samples of the Wasamac deposit

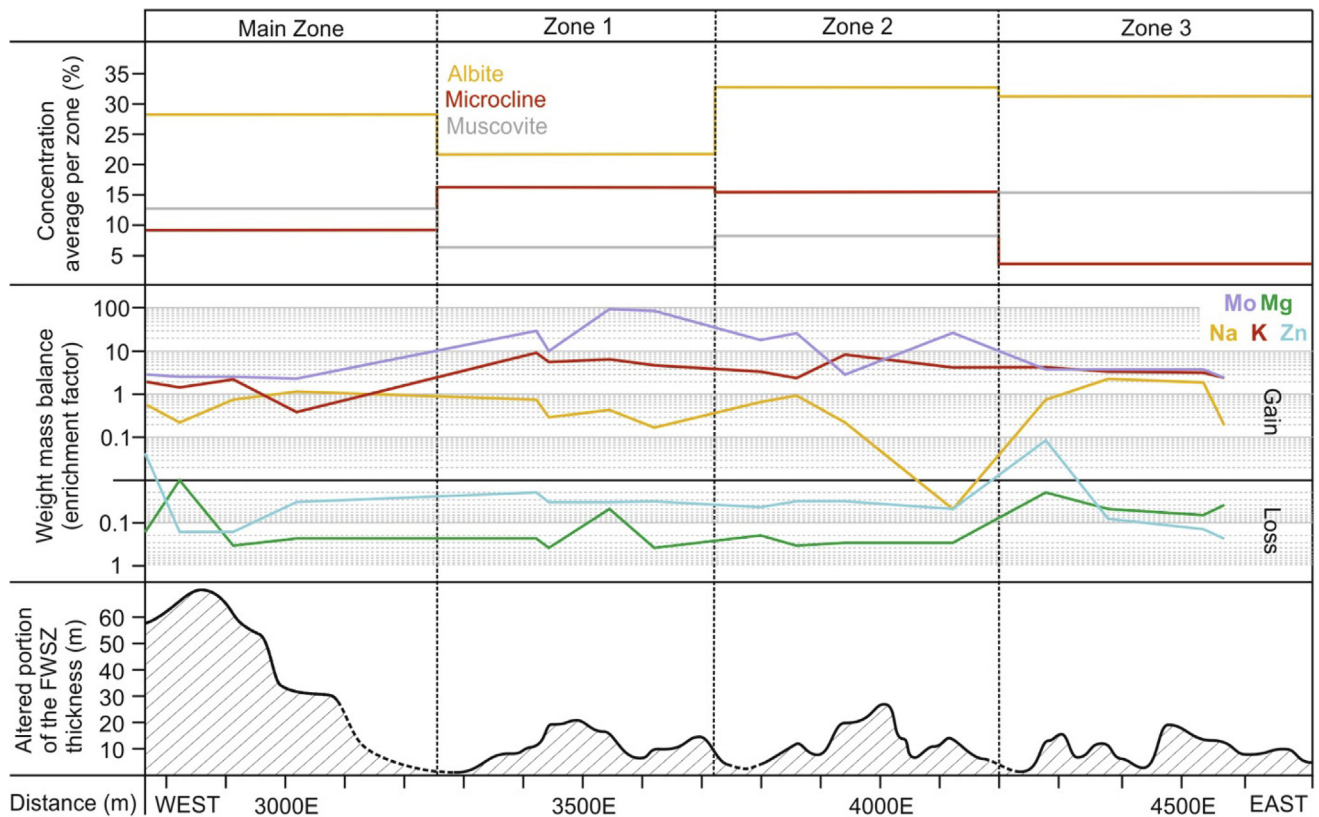


Fig. 9. Longitudinal summary of alteration mineralogy and mass balance calculations from Wasamac deposit's four mineralized zones. These samples were selected from the 16 samples described in the sampling and analytical methods section. The thickness of altered and mineralized faulted units is also represented. An enrichment factor of 1 means a 100% gains from the unaltered protolith, mass gain for the associated element is thus twice as the original mass.

display a tholeiitic to calc-alkaline signature. The altered samples show two alkaline trends, proportional to the intensity and characteristics of the two alteration facies (Fig. 7C). The variations in SiO_2 concentration may be attributed to the abundance of irregularly distributed millimetric to sub-millimetric veinlets locally associated with potassic-altered units. Grant isocons (Grant, 1986) and mass balance calculations show similar results for both alteration facies (Fig. 8A, Fig. 8B). Potassic alteration displays strong enrichments in W, Pb, Bi, Te, Mo, Ag and Au, minor enrichment in As, variable enrichment in Cu, and depletion in Zn, Mg and V (Fig. 8B). Albitic alteration shows similar gains and losses, but to a lesser degree (Fig. 8B). Tungsten mass gains are greater for the albitic alteration assemblage than for the potassic assemblage.

At the scale of the Wasamac shear zone, potassic and albitic alteration assemblages show regional zoning along the longitudinal axis of the shear zone, in which potassium mass gains are stronger in the central part (Fig. 9). This enrichment is linked to microcline crystallization, which is typical of the early stage of hydrothermal activity that is well preserved in Zones 1 and 2. These zones are characterized by consistently strong gains in molybdenum accompanying the potassium gains. Potassium enrichment is also strong in the Main Zone and Zone 3 where it is related to sericite crystallization in the albitic assemblage (Fig. 9). Sodium enrichment varies strongly in Zones 1 and 2 where albitic alteration may be locally absent (Fig. 4A). The Main Zone and Zone 3 are typically more enriched in sodium and less enriched in potassium.

5. LA-ICP-MS characterization of pyrite zonation

Thirteen samples of pyrite were selected for LA-ICP-MS investigations from typical potassic and albitic alteration facies in the

Main Zone and Zone 2. Although pyrite occurs as small grains in the two alteration assemblages, it frequently displays zonation with spongy cores and clear secondary overgrowths. Four crystallization stages can be distinguished.

The inner core (stage 1 pyrite), rarely preserved, appears as anhedral pyrite with nonporous texture. Despite traces of As, Pb, Se, Bi, Ba, Ti and V, this first stage of crystallization does not host gold or any significant metal enrichment. The second crystallization phase (stage 2 pyrite) is represented by porous pyrite carrying gold. Generally euhedral, the cavities of this pyrite generation are often filled with gold tellurides, titanite, silicates, hematite and chalcopyrite (Fig. 10). The pyrite lattice is enriched in Ag, Au, Te, Pb, Bi, Cu +/- Zn, Co, Ti, Ba and As. According to SEM observations, most of this gold enrichment occurs as invisible particles. Gold-bearing phases incorporated into the lattice of stage 2 pyrite may thus be sub-micron in size. Enrichment in Cu and Ti is sporadic, with strong values coinciding with chalcopyrite and titanite inclusions (Fig. 10). According to microscopic observations on 22 samples, stage 1 and 2 pyrites occur in both alteration facies, but are more abundant in the potassic assemblage than the albitic assemblage. The third phase of crystallization (stage 3 pyrite) displays clear textural overgrowths, and is the predominant pyrite generation in pyrite-rich albitic alteration. This stage is composed of euhedral pyrite, generally poor in trace elements. Stage 3 pyrite locally carries large chalcopyrite inclusions and shows scarce micron-scale amygdaloidal-shaped voids. Rare micron-scale gold telluride inclusions are locally associated with this crystallization episode. Successive bands characterized by variable Ni, Co and As concentrations are associated with this overgrowth stage. Nickel-cobalt zonation is observed, and the concentrations of these elements show a negative correlation. The fourth stage is

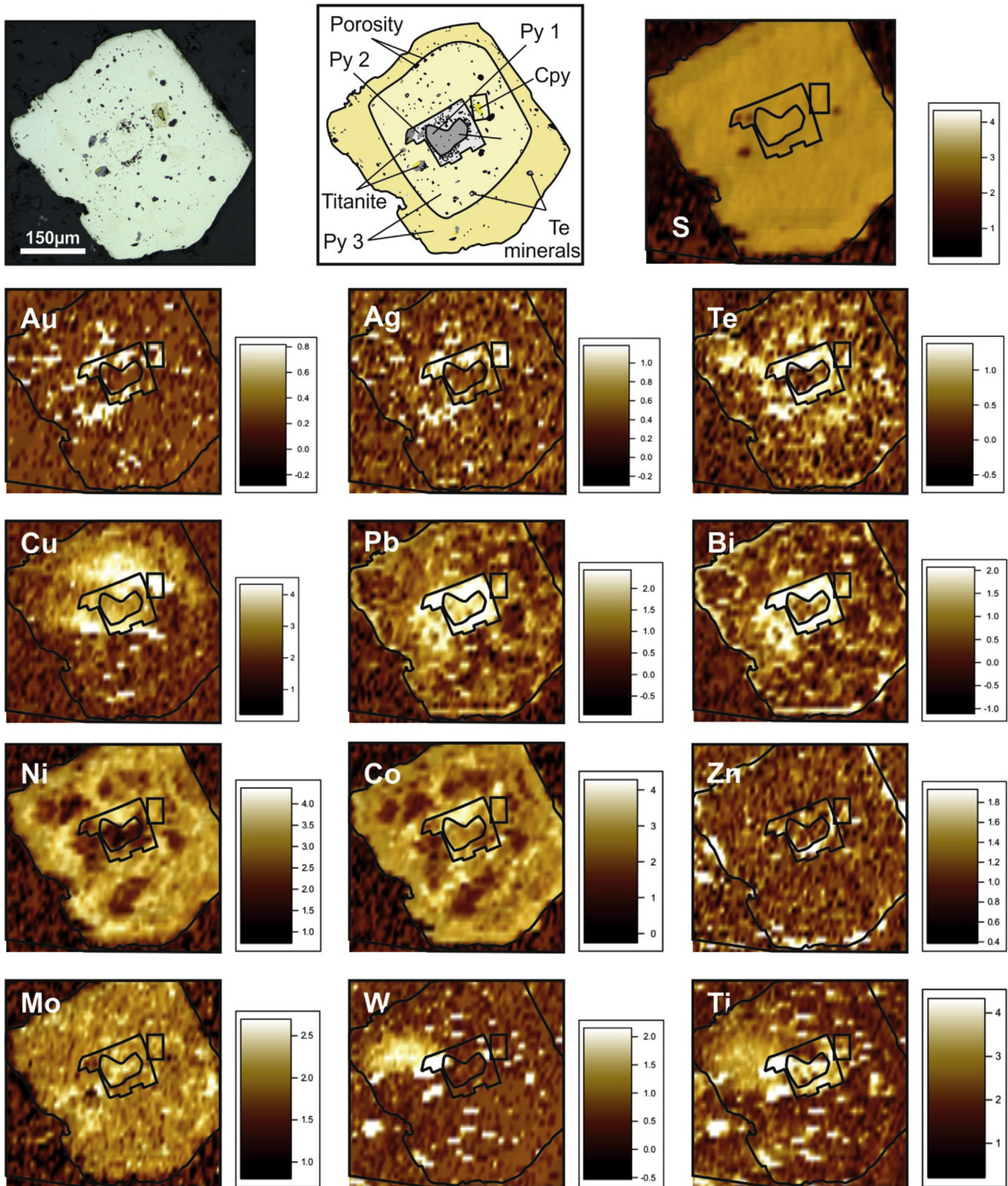


Fig. 10. LA-ICP-MS maps of a pyrite grain from the Main Zone displaying pyrites stages 1 to 3. From the top left to the bottom right: photograph of targeted pyrite in reflected light microscopy displaying varying concentric textures, schematic interpretation of pyrite zonation, LA-ICP-MS maps of S, Au, Ag, Te, Cu, Pb, Bi, Ni, Co, Zn, Mo, W, Ti. The legend for LA-ICP-MS colorations are \log_{10} ppm.

characterized by the fracturing of pyrite overgrowths but did not involve pyrite crystallization. This brittle tectonic event is mainly documented within albitic alteration zones where gold is most frequently observed as free native gold. The infilled fractures are enriched in Cu, Pb, Bi, Ti, Zn, V, Ag, Au and Te (Fig. 11). Late metal

enrichment is locally observed in stage 3 pyrite rims, featuring Pb, Bi \pm Ni, Au, Ag, Te (Fig. 10).

The earliest stage of gold mineralization is associated with spongy stage 2 pyrite (Fig. 12). This pyrite stage is predominant in the potassic facies, but less significant in the albitic facies. This

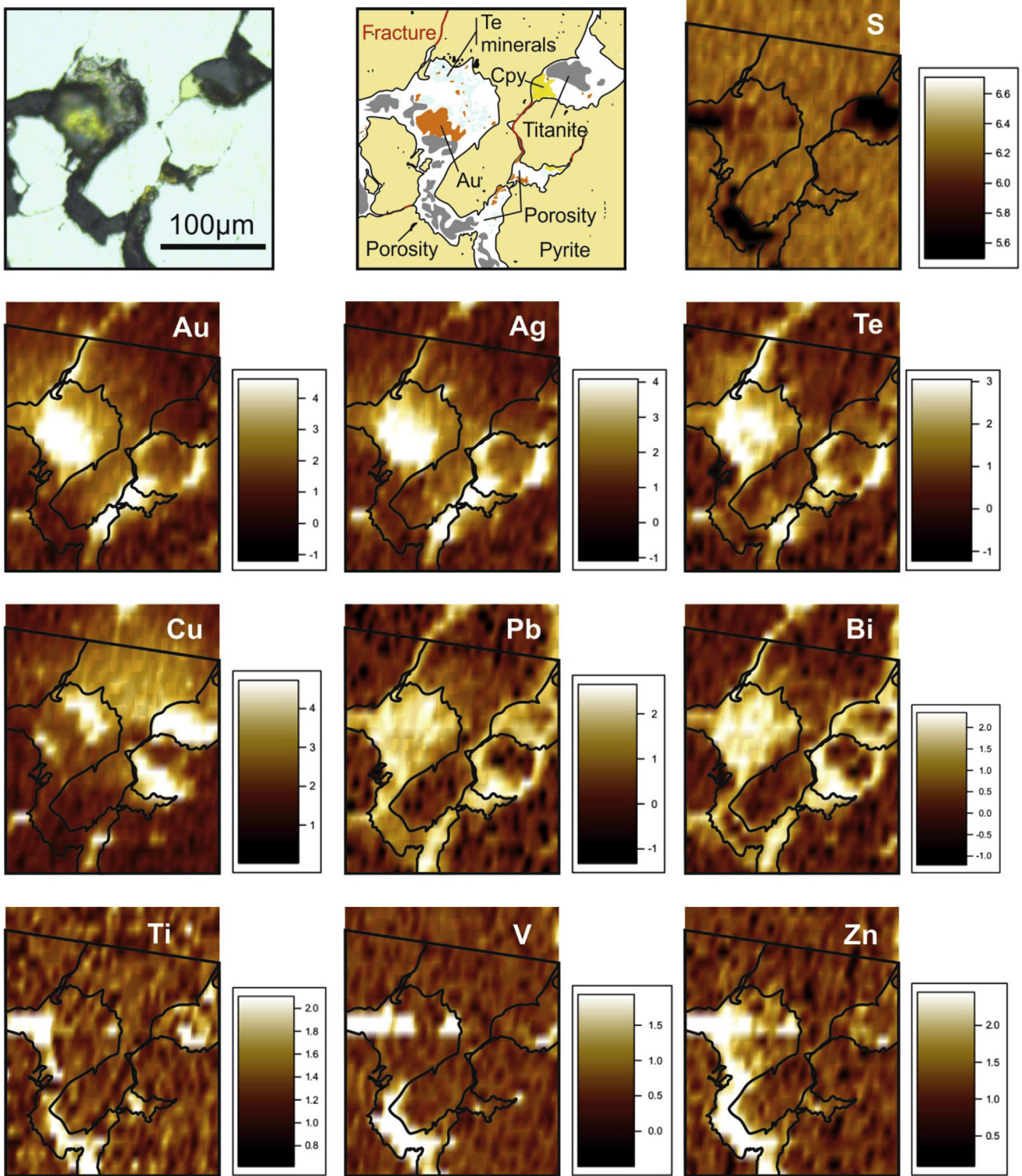


Fig. 11. LA-ICP-MS maps of a fractured pyrite grain from the Main Zone. From the top left to the bottom right: photograph of targeted pyrite in reflected light microscopy, schematic interpretation of the photograph, LA-ICP-MS maps of S, Au, Ag, Te, Cu, Pb, Bi, Cu, Ti, V, Zn. The legend for LA-ICP-MS colorations are log(10) ppm.

observation correlates with those made at the scale of the deposit, where 70% of the gold is described as trapped in pyrites in the potassic assemblage dominating Zones 1 and 2, compared to an average of 50% of gold in the dominant albitic assemblage of the Main Zone and Zone 3 (Fig. 5). High concentrations of Te-Ag-Au in the early gold-rich pyrites of the potassic facies, as determined by LA-ICP-MS, also correlate with the preferential concentration

of telluride minerals on a larger scale in Zones 1 and 2 (Fig. 5). Furthermore, mass balance calculations show higher mass gains for the same elements in potassic-altered rocks compared to those affected by albitic alteration (Fig. 8A and B). The fourth stage, described as the brittle event affecting stage 1 to 3 pyrites, also hosts gold mineralization. It is most often observed in the albitic alteration assemblage, where gold occurs mainly as free native

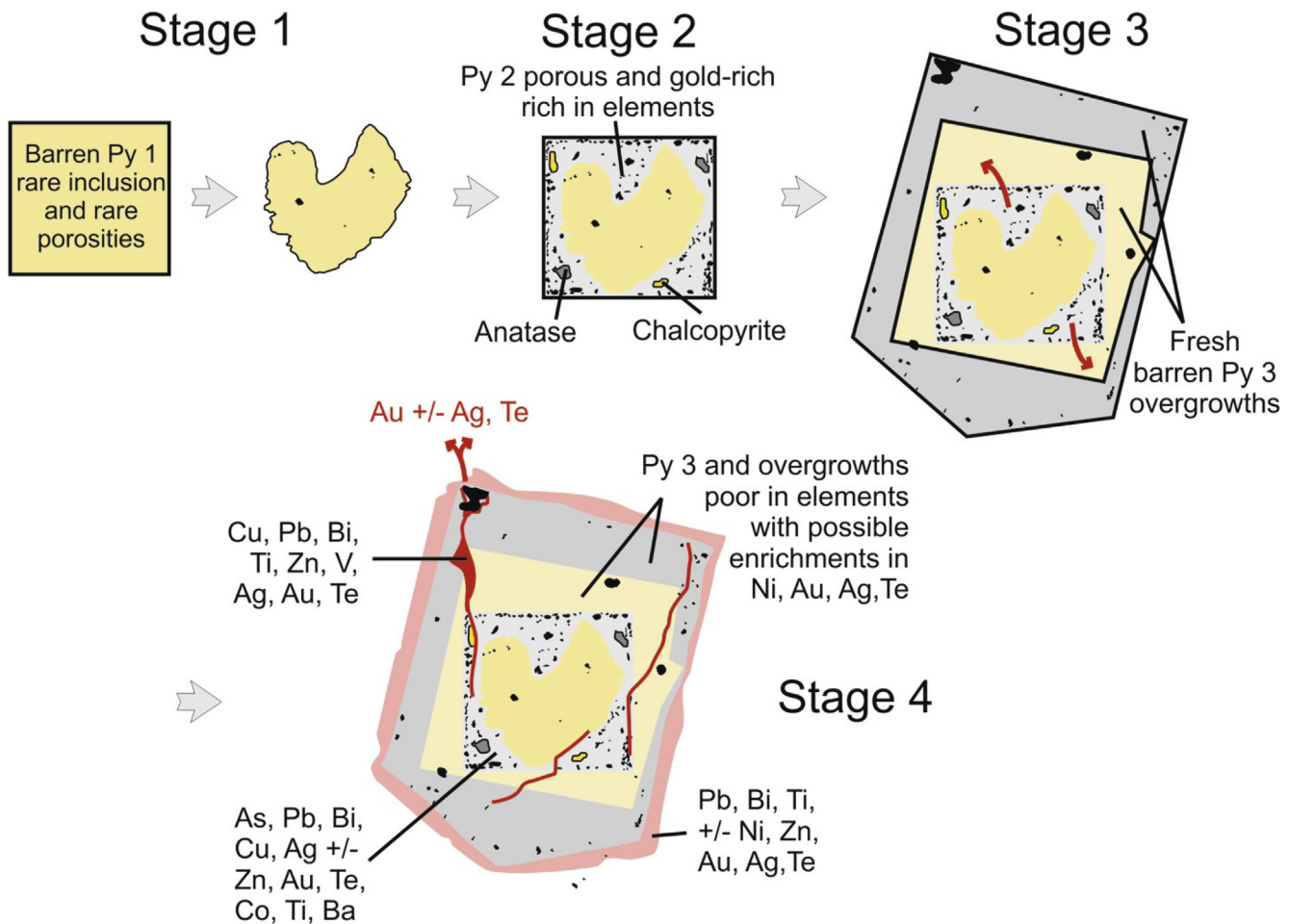


Fig. 12. Schematic model of pyrite zonation and metallic anomalies observed with LA-ICP-MS analyses. This model represents a composite interpretation from thirteen LA-ICP-MS maps. Four events are observed: three pyrite overgrowths and a late fracturation event. Gold is related to the porous pyrite overgrowth (stage 2) and may be associated locally to the phase 3 overgrowths by scavenging the pyrite stage 2. The fracturation event is represented with the red irregular lines. A pink coloration represents chemical anomalies frequently observed enclosing pyrite rims (observed with Pb and Bi in Fig. 10).

gold. This event has also been observed in brecciated potassic-altered rocks. Even though pyrite zonation is unevenly distributed in the potassic and albitic assemblages, all four stages were identified in both alteration facies.

6. Discussion

6.1. The Wasamac deposit: An early hydrothermal gold enrichment with a magmatic affinity

6.1.1. K-feldspar hydrothermal alteration signatures

The early oxidized potassic assemblage identified at the Wasamac deposit, mainly in its core zones, represents an uncommon hydrothermal signature among examples of Archean orogenic gold mineralization. Gold is associated with the crystallization of microcline, sericite, carbonates and pyrite, rather than that of biotite, amphibole and pyrrhotite, the latter reflecting typically higher temperature than pyrite-rich environments (Cassidy and Bennett, 1993; McCuaig and Kerrich, 1998). This reveals that upper greenschist facies conditions were not reached during this hydrothermal event, and consequently that potassic alteration was in broad thermal equilibrium with the wall rocks.

Under greenschist grade conditions these characteristics are most commonly reached proximal to or within a large number of variably oxidized felsic and alkaline intrusions (Colvine et al.,

1988; McCuaig and Kerrich, 1998). Numerous examples among gold belts around the world exhibit similar alteration patterns, such as the southern New England Fold Belt (Australia), the Tintina and Tombstone-Tungsten gold belts (Canada, USA), the Tian-Shan Belt (Kazakhstan, Uzbekistan), and the Inner Mongolia Axis in China (Thompson et al., 1999; Lang and Baker, 2001; Blevin, 2004; Cook et al., 2009; Goldfarb and Groves, 2015). In the Abitibi Greenstone Belt, gold-rich oxidized potassic alteration developed in the Malartic, Beattie and in Kirkland Lake district deposits (Robert, 2001; Hart, 2005; Ispolatov et al., 2008; Helt et al., 2014; Bigot and Jébrak, 2015; De Souza et al., 2015). It has also been recognized at the Baie Renault Syenite near Wasamac, located about 5 km west of the Francoeur deposit (Legault and Rabeau, 2007). However, such hydrothermal alteration is rarely observed away from syenitic intrusions. The metal trends characterizing this alteration assemblage (strong enrichment in W, Pb, Bi, Te, Mo and Ag, minor enrichment in As, variable enrichment in Cu, and depletion in Zn, Mg and V) share similarities with regional syenite-related deposit signatures, such as those of the Kirkland Lake district (Ispolatov et al., 2008). They however contrast with the neighbouring Fortune Lake and Astoria orogenic gold deposits, which are characterized by different metallic signatures such as Mn, Co, Ni, Cu, Zn, As, Sb, Pb, Bi (Rafini, 2014; Laporte, 2016).

Despite the strong alkaline intrusion-related affinity of the early stage of hydrothermal alteration, syenite dykes in the immediate

vicinity of the Wasamac deposit are barren and display no clear evidence of a genetic relationship with mineralization. However, the presence of a pyrite-rich syenite dyke carrying 100 ppb Au adjacent to the Francoeur ore body suggests that the emplacement of a syenite intrusion may have played a role in gold enrichment along the FWSZ. It is thus possible that some of the particular characteristics at the Wasamac deposit are related to an early episode of gold enrichment associated with the emplacement of a gold-enriched syenitic intrusion, such as the widespread mineralized syenitic systems recognized in the Kirkland Lake district to the west.

6.1.2. Early gold mineralization

The pyrite textures and trace element zonation patterns suggest a multistage process of ore genesis at the Wasamac deposit. The earliest gold occurred as telluride micro-inclusions in the lattice of micron-scale porous stage 2 pyrite in potassic alteration assemblages. This auriferous stage of pyrite growth is the only one with a porous texture and high concentrations of metals (Fig. 12), implying specific hydrothermal conditions. Putnis (2002) related such textural characteristics in pyrite to a coupled dissolution-recrystallization process. Recent studies using the LA-ICP-MS technique on pyrites displaying similar textural characteristics to those at Wasamac provided additional data in support of early gold-rich dissolution-recrystallization processes (Cook et al., 2009; Zhao et al., 2011; Zhang et al., 2014). Stage 2 pyrite may thus be related to two successive hydrothermal events: (1) partial dissolution of barren stage 1 pyrite under oxidizing conditions; and (2) crystallization of stage 2 pyrite during a mineralized hydrothermal event, trapping inclusions of oxide minerals, sulfides and tellurides.

Except for rare occurrences of coarse remobilized native gold in quartz veins, gold mineralization in the potassic alteration assemblage cannot be detected by reflected light microscopy or the SEM. However, LA-ICP-MS analysis did reveal high gold values within all unfractured porous stage 2 pyrites, consistently accompanied by Te and Ag. Gold trapped in sulfides has been documented as lattice-bounded nanoparticles and as micro-inclusions in As-rich sulfides for various styles of mineralization in the Abitibi Greenstone Belt and around the world (Cabri et al., 1989; Bonnemaïson and Marcoux, 1990; Cook and Chrysoullis, 1990; Fleet et al., 1993; Large et al., 2007, 2009; Cook et al., 2009; Bigot and Jébrak, 2015). Cook et al. (2009) and Ciobanu et al. (2012) described gold-rich As-free sulfides, suggesting that As is not an essential component for incorporating gold within the pyrite lattice, and that Te may distort the lattice allowing Au to enter. On this basis, it would seem that most of the early gold at Wasamac occurs as invisible lattice-held telluride phases in pyrite that crystallized during potassic hydrothermal alteration.

6.2. The Wasamac deposit: Structural and hydrothermal overprint and gold remobilization

6.2.1. Albitic hydrothermal alteration signature

In the Wasamac deposit, the late albitic hydrothermal signature overprints both the earlier potassic alteration and unaltered intermediate to felsic host rocks. The metal assemblage in the albitic facies at Wasamac is similar to that of the potassic facies but contains smaller amounts of Mo, Te, Pb +/- Bi with locally higher W, Au and Ag. This may be due to hydrothermally induced losses and concentrations from the earlier potassic assemblage, or it may indicate a new hydrothermal metal event with similar characteristics. Albite is a common alteration mineral described within or immediately adjacent to Archean gold mineralization systems (Colvine et al., 1988). A strong sodium enrichment may be related to four potential sources: (1) the hydrolysis of alkali feldspar, (2) the breakdown of plagioclase feldspar, (3) sea water contamination

rich in chlorides, which improve metal mobility, (4) albite-rich magma and associated hydrothermal circulation resulting from fractional crystallization, possibly genetically related to the same magmatic source that produced the potassic alteration (Kishida and Kerrich, 1987; Colvine et al., 1988; Witt, 1992; Smith et al., 1993; Gammons and Williams-Jones, 1995; McCuaig and Kerrich, 1998; Robert, 2001; Neumayr et al., 2008).

Along the CLLFZ, albitization is commonly observed as pervasive hydrothermal replacement in greenschist rocks in several contexts, including: (1) brittle-ductile fault zones (e.g., the Lapa mine; Simard et al., 2013), (2) in contact with veins (e.g., the Sigma-Lamaque mines; Robert and Brown, 1986b), (3) as flow-ore alteration (e.g., the Kerr-Addison district; Kishida and Kerrich, 1987; Smith et al., 1993), and (4) as albitite dykes (e.g., the Francoeur deposit; Couture and Pilote, 1993). In the Kirkland Lake gold district, gold-rich albitized zones are spatially associated with syn- to post-tectonic alkaline intrusions (Ispolatov et al., 2008). Closer to the Wasamac deposit there is a spatial relationship between gold and albitite dykes at Francoeur and Kerr-Addison. Mineralization at Kerr-Addison has been interpreted to be genetically related to an alkaline intrusion buried at depth beneath the shear zone (Smith et al., 1993). Numerous authors, including Kishida and Kerrich (1987), Witt (1992), Smith et al. (1993), Robert (2001) and Lang and Baker (2001) and Neumayr et al. (2008), pointed out the nearly ubiquitous spatial association of albitization with intrusion-related gold systems, and suggested that felsic/alkaline intrusions could cause both potassic and albitic hydrothermal alteration. Moreover, the dominance of albite over sericite in albitic alteration facies has often been documented at intrusion-related gold deposits, in contrast with the prevalence of sericite over albite in orogenic gold deposits (Robert, 2001).

However, the similar metallic composition described in the albitic alteration assemblage, such as the coeval crystallization of low metal content pyrites stage 3 suggest a metallic inheritance from the early potassic hydrothermal event to the albitic one. Such argument supports that albitization would be the result of *in situ* metasomatism, amongst which albite would be generated by the hydrolysis of alkali feldspar from the previous assemblage by contrasting reduced fluids (Colvine et al., 1988). Besides, this hydrothermal episode is coeval with a structural activity inducing the brecciation of potassic-altered units (Fig. 4E) and ultimately controlling gold characteristics.

The methods of investigation developed in this study do not provide an absolute conclusion, as both metamorphic and magmatic fluids can generate such alteration pattern. However, the characteristics associated with the albitic assemblage suggest that tectonics triggered the second hydrothermal activity. Such setting, typical of orogenic gold systems, is most frequently associated with fluids related with a metamorphic affinity. Further investigations on mineralized fluids at the Wasamac deposit would bring valuable information on a possible magmatic connection and help discriminating both hydrothermal events, contributing in the understanding of regional gold mineralization environments.

6.2.2. From trapped invisible tellurides to free native gold

Stage 1 and 2 pyrites in the potassic facies are rarer in the albitic facies, which features a high concentration of larger stage 3 pyrite overgrowths and subsequent stage 4 cataclasis. The stage 3 overgrowths are composed of nonporous pyrite with only locally enrichments in Ni, Co and As, and local chalcopyrite inclusions. Stage 3 and 4 pyrites are frequently observed in the albitic assemblage that fills fractures in potassic-altered rocks or as the supporting matrix to potassic breccia clasts, which are otherwise devoid of these stages. Stage 3 pyrite, coeval with albitization, thus reflects changes in hydrothermal conditions within the FWSZ. Furthermore, the lack of metals in these large pyrite overgrowths supports



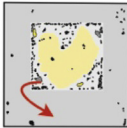
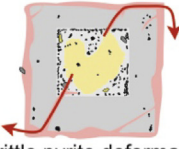

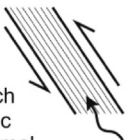
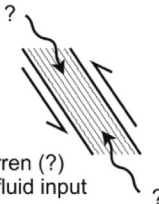

Structural features	- S1 main foliation and local S2 ductile deformation creation and maintenance		- Brecciation of K-feldspar altered units - Structural partitioning	- Brecciation of K-feldspar altered units - Pyrite fracturation
Alteration chemistry	- Regional metamorphic signature - Carbonate veinlets towards the strain zone	- Red potassic pervasive alteration - K ₂ O, K, Mo, W, Pb, Bi strong values - Strong red-ox variations	- Greyish-beige albitic pervasive alteration overprinting K-altered units and fresh metavolcanic rocks - Na ₂ O, Na, Cu, W, Pb, and Bi strong values	- Greyish-beige albitic pervasive alteration - Na ₂ O, Na, Cu, W, Pb, and Bi strong values
Gold characteristics	None	- Invisible gold telluride minerals trapped in spongy pyrite structure - Few visible gold telluride inclusions in pyrite	- Recycling gold material from gold-rich pyrite - Possible new gold input	- Abundant gold tellurides and native gold filling pyrite fractures, ultimately released in the alteration assemblage - Gold tellurides <5µm free native gold >5µm
Pyrite chemical enrichments	- Fluctuating Ni and Co enrichment - Few inclusions and porosities	- Cu, Zn, Pb, Bi, Co, Ag, Te, Au - Prevalent anatase, hematite and chalcopyrite inclusions	- Fluctuating Ni and Co enrichment - Few inclusions and porosities - Local gold-tellurides inclusions	- Pb, Bi, Ti, Zn, Cu, Au +/- Te, Ag - Late metal enrichments remobilizations along fractures and around pyrite
Pyrite textural characteristics	 Crystallisation of barren pyrite stage 1	 - Dissolution-recrystallization process - Gold-rich spongy pyrite stage 2	 Pyrite stage 3 crystallisation Local gold recycling	 Brittle pyrite deformation Native gold release (stage 4)
Proposed model of tectonic and hydrothermal activity	 Initiation of reverse ductile faulting	 Gold-rich potassic hydrothermal input	 Barren (?) sodic fluid input	 Gold evolution and remobilization

Fig. 13. Schematic interpretation of Wasamac deposit's hydrothermal and tectonic processes associated with gold mineralization. Gold rich porous pyrite (stage 2) is associated with the early potassic hydrothermal event. A second hydrothermal phase follows crystallizing pyrite stage 3 during the albitic alteration. Thirdly, the maintenance of tectonic activity fractured previous pyrite overgrowths. This late tectonic activity is proposed to be associated with the gold remobilization and concentration.

a barren albitic hydrothermal event. These features may indicate crystallization from metamorphic fluids that scavenged metals with less alkaline affinities from the host rocks.

The late stage 4 brittle event caused the fracturing and cataclasis of previous generations of pyrite. This event is mainly represented in the albitic alteration assemblage containing free gold grains and rare gold tellurides. The pyrite fractures are commonly filled by gold-bearing phases or native gold (Fig. 6B and E). Pyrite fracturing may thus represent a critical feature for concentrating gold. [Bonnemaison and Marcoux \(1990\)](#), [Mumin et al. \(1994\)](#) and [Genkin et al. \(1998\)](#) and [Morey et al. \(2008\)](#) proposed that the superposition of structural events controls the recrystallization of pre-existing gold mineralization in orogenic gold deposits. According to [Morey et al. \(2008\)](#) study on the successive structural destabilization of the early stages of gold-rich pyrite and arsenopyrite, gold tends to recrystallize and concentrate, resulting in overall gold enrichment. Most recently, [Bigot and Jébrak \(2015\)](#) described a similar

structural control on gold chemistry at the syenite-related Beatie deposit. At the Wasamac deposit, the size of pyrite fracture planes seems to control gold mineralogy, with tellurides filling fractures <5 µm wide, and native gold filling larger fractures. Invisible occurrences of metals in stage 2 pyrite may have been extracted during the stage 4 fracture event because Au, Ag, Te, Pb, Bi and Ti are found in high concentrations in the material filling the fractures and in the fractured pyrite rims (Fig. 11).

Stage 4 pyrite paragenesis with respect to alteration assemblages and pyrite zonation suggests that the brittle event controlled gold extraction from the lattice of early porous pyrites. The increasing size of gold grains and progressive chemical loss of Te and Ag from the potassic to albitic assemblages likely reflect the maturation process of gold linked with a tectonic overprint. The gold stock associated with the albitic alteration may be the result of a structural concentration process involving early pyrite-hosted mineralization; however, a second hydrothermal mineralized event cannot be ruled out (Fig. 13).

	Kirkland Lake deposits	Kerr-Addison	Francoeur	Wasamac	Lapa	Malartic	Sigma-Lamaque
Host lithology	Ultramafic, tholeiitic and calc-alkaline meta-volcanic units Conglomerates and sandstones Three-phase syenitic intrusions	Ultramafic meta-volcanic units Tholeiitic mafic units Inter-bedded sediments	Meta-andesite Albitite dykes	Meta-andesite	Ultramafic and mafic volcanic units Graywacke	Porphyritic monzodiorite Metasedimentary units Mafic-ultramafic units	Andesitic flows and volcanoclastic rocks Porphyritic diorite
Host structure(s) Distance CLLFZ	CLLFZ and subsidiary second order fault zones Mostly Au-bearing veins Less Au-bearing sulphides in disseminated altered faulted units	CLLFZ and second order Kerr Fault, similarly striking Au-bearing veins Au-bearing sulphides in disseminated altered mylonite	Second order FWSZ, 2km north of the CLLFZ Disseminated Au-bearing sulphides and free native gold grains in altered mylonite	Second order FWSZ, 2.5km north of the CLLFZ Disseminated Au-bearing sulphides and free native gold grains in altered mylonite	CLLFZ Au-bearing sheared veinlets within brittle-ductile to ductile conditions	CLLFZ and proximal subsidiary fault Au-bearing veins	3.5km north of the CLLFZ along subsidiary faults Brittle vein system
Alteration mineralogical characteristics	Qtz, ser, carb, K-feldspar, alb, py Post-ore chlorite fault gouge	Four alteration assemblages: (1) Qtz, chlo, carb, ser, alb, py (2) Qtz, carb, fusch (3) Alb, musc, chlo, py (4) Graph, py	Three alteration assemblages: (1) Pre-ore: Alb, carb, hem, ser, qtz (2) Alb, carb, py, ser (3) Post-ore: sulfate-bearing veinlets	Two gold-rich alteration assemblages: (1) K-feldspar, ser, carb, qtz, hem, py (2) Alb, ser, carb, chlo, py	Qtz, dol, cal, biot, musc	Pervasive potassic alteration (K-feldspar and biot), carb, py, and local qtz within host lithologies	Qtz, trm, carb, cho +/- alb, schee
Alteration geochemistry and additional informations	Strong mass gains in K and Na	Polyphased alteration events and overprinting Mass gains in K, Ca, Cu, Ag, W, Au, Ag Variable gains/losses in Na	(1) Mass gains in K ₂ O, Rb, W, Co ₂ , Au, S (2) Mass gains in Na ₂ O, W, Au, S, Co ₂	(1) Mass gains in K, Mo, W, Pb, Bi, Te, Ag, Au (2) Mass gains in Na, Mo, W, Pb, Bi, Te, Ag, Au	Superposition of three metamorphic episodes (1) syn-ore biot. alteration (2) hornb, oligo prograde metamorphism (3) Act. alb, retrograde metamorphism	Mass gains in K, S, Ag, Te and Au, significant gains in Sb, W, Bi and Pb. Significant mass loss in Cu	Zoned alteration haloes extending up to several meters away from the veins with ser, carb, py, alb.
Mineralization mineralogical characteristics	Py + minor cpy, moly, sph Spatially associated with faulted syenitic intrusions Gold closely associated with tellurides	Gold bearing disseminated pyrite in (1) and (3) Free native gold grains in veins and veinlets in (2) Gold-rich sulphide remobilizations in (4)	Gold associated with As-free pyrite and free native gold grains	(1) Telluride gold minerals associated with As-free zoned pyrite (2) Disseminated free native gold grains	Finely disseminated auriferous apy, po +/- py Native gold disseminated in altered wall rocks	Mainly native gold and subordinate gold tellurides Spatial association with Pyrite and minor Cpy, Ga, Sph, Hm, Mo and Ag-Pb-Bi Tellurides	Py +/- po Native gold and gold tellurides in veins with crack ad seal texture
Mineralization complementary informations	High Te, Au, Mo, Pb, Ag Sporadic Cu Low As High Au/Ag	Event (3) : Gold-bearing pyrites associated with 5 000 albitite dykes High Au/Ag	Metallic signature: W, Te, Bi, Cu, Pb, Ni, Zn High Au/Ag	Chemical control of gold precipitation in (1), structural control of gold recrystallization in (2) Gold mineral maturation from (1) to (2) High Au/Ag	Characteristic Au, Sb, As and Au, As associations Early low grade mineralization (1), remobilized (2) and native gold precipitation (3)	Au concentrated in two generations of discontinuous veins, and within the alteration envelopes Au deposition related to pyritization followed by oxydation events	Metallic signature: Te, B, S, Ag
Genetic interpretation	Magmatic-hydrothermal genetic model Syenite-related overprinted by regional deformation	Orogenic gold deposit resulting of repeated cycles of hydraulic fracturing Possible genetic association for gold-bearing albitites with buried alkaline stock	Orogenic gold deposit Fluid/rock interaction between pre-ore oxidized dykes acting as a trap for gold-bearing pyrite crystallisation	Magmatic-hydrothermal genetic model Biphased alkaline hydrothermal circulation within orogenic structure possibly intrusion-related	Orogenic gold deposit associated with a polyphased metamorphic control on gold enrichment	Magmatic-hydrothermal genetic model "Oxidized" intrusion-related structurally-associated	Late brittle orogenic gold deposit within a shear-zone Possibly related to late diorite-tonalite plugs

Fig. 14. Descriptive comparison between several gold deposits situated along the CLLFZ. Qtz: quartz, Chlo: chlorite, Ser: sericite, Carb: carbonates, Alb: albitite, Dol: dolomite, Cal: calcite, Trm: tourmaline, Schee: scheelite, Biot: biotite, Fusch: fuschite, Musc: muscovite, Py: pyrite, Po: pyrrhotite, Cpy: chalcopyrite, Moly: molybdenite, Sph: sphalerite, Apy: arsenopyrite, Hm: hematite, Ga: galena. (Ispolatov et al., 2008; Kishida and Kerrich, 1987; Smith et al., 1993; Couture and Pilote, 1993; Simard et al., 2013; Helt et al., 2014; Poulsen et al., 2000).

6.3. Genesis of the Wasamac deposit

According to this study and by comparison with similar results from other deposits regionally and around the world, a genetic model including a two-step gold enrichment process is proposed. First, an early magmatic-hydrothermal event crystallized gold as invisible sulfide-bound gold tellurides. This first episode may be linked to a deep-seated alkaline intrusion buried beneath the FWSZ. Secondly, one or more structural events brecciated the potassic-altered units and generated an albitic hydrothermal overprint under reduced conditions, crystallizing nonporous barren pyrites. Thirdly, renewed – or sustained – faulting preferentially localized in the less competent albitized units progressively remobilized gold from the early pyrite lattice along fractures, ultimately releasing gold as larger free native grains along with other metals previously held in the pyrite lattice.

This structural control on gold represents a typical feature of gold mineralization in orogenic settings (Bonnemaison and Marcoux, 1990; Mumin et al., 1994; Genkin et al., 1998). Overlapping structural events inducing gold liberation from invisible sulfide lattice-held occurrences into native free gold grains has been observed at several deposits analogous to Wasamac. Such mineralization features were described at the Beattie deposit in the Abitibi (Bigot and Jébrak, 2015), within deposits from the Boorara and Bardoc Fault Zones in the Eastern Gold Fields of Western Australia (Morey et al., 2008), and at the Dongping, Huangtuliang and Hougou deposits in the North China Craton (Cook et al., 2009). However, Oliver (1996) postulated that changes in gold grain size and mineralogy during fracturing could reflect two distinct genetic processes: one occurring in

an open system involving a new fluid, and the other in a closed system through the reworking and concentration of pre-existing metals. It is thus possible that gold at Wasamac was the product of the early potassic event only, or both the potassic and the albitic hydrothermal events.

Despite the conspicuous structural control of ore at the Wasamac deposit, comparisons with other deposits along the CLLFZ support the hypothesis that the early characteristics described at Wasamac display stronger similarities with syenite-related systems than orogenic systems (Fig. 14). In the same way that Robert (2001) used the similar dual mineralization characteristics at the Francoeur deposit as a basis for questioning its classification, the similar two styles of gold mineralization at Wasamac, also make it difficult to classify. Such ambiguity is evident at the regional scale, where deposits to the west display irregular and locally overlapping mineralization styles, likely representing up to four hydrothermal/structural events (Kishida and Kerrich, 1987; Smith et al., 1993; Robert, 2001; Legault and Rabeau, 2007; Ispolatov et al., 2008). However, the crosscutting relationships between the two styles of gold mineralization at Wasamac bring new insights for the successive contribution of intrusion-related and orogenic gold environments, clarifying its classification.

By comparing observations presented in this study to previous studies on neighbouring deposits along the western part of the CLLFZ, a progressive greater alkaline magmatic contribution from the Wasamac deposit towards the Kirkland-Lake gold district can be noticed. It would appear that mineralization facies deepen to the west. Since metamorphic grade does not increase westward, the change in mineralization facies may be related to a change in the depth of magma chambers.

7. Conclusions

The Wasamac deposit is a replacement-type gold deposit located along a second-order ductile fault zone. It is the result of two successive alkaline hydrothermal events, potassic then albitic. Each alteration facies is marked by pyrite crystallization and gold concentration. Four features characterize gold mineralization at the Wasamac deposit: (1) it is disseminated within the FWSZ mylonitic schist, without any lode systems, (2) As-free pyrite is the only sulfide spatially associated with gold mineralization, (3) pyrite zonation supports metal inheritance from one hydrothermal event to the other, and (4) gold mineralogy is specific to each alteration facies. The LA-ICP-MS data showed a correlation between gold concentration and the textural characteristics of pyrite.

Gold first occurred as visible and invisible telluride minerals crystallized in the lattice of stage 2 pyrite. This early event was coeval with potassic hydrothermal alteration. Based on the intense hematization of the potassic assemblage and the textural characteristics of stage 2 pyrite, the gold precipitation process would have occurred under different oxidation conditions, inducing a dissolution-recrystallization process. Following this input of mineralizing fluid, hydrothermal activity then crystallized metal-poor stage 3 pyrite contemporaneously with the albitic alteration assemblage. This second hydrothermal activity occurred under reducing conditions. Through structural partitioning, the albitic alteration assemblage became more deformed than the earlier potassic assemblage. However, potassic-altered rocks were locally brecciated, preferentially along their contacts with the albitic assemblage. This subsequent deformation preferentially overprinting the albitic assemblage caused the fracturing of pyrite. Spatially associated with disseminated native gold, this late brittle event may have caused the progressive extraction of gold from early stage 2 pyrite. Gold evolution, beginning as telluride crystallized in thin fractures, and then as native gold in larger fractures, liberated as native gold grains in the albitic alteration mineral assemblage. This structural control on gold concentration is characteristic of processes involved in orogenic-type gold deposits.

The Wasamac deposit may thus represent the superposition of two hydrothermal events, one related to alkaline magmatism and the second to remobilization by “orogenic-style” hydrothermal fluids. Genetically, we suggest that early ore fluids were derived from a deep-seated source involving magmatic-hydrothermal processes followed by a structural overprint and associated remobilization of gold.

Acknowledgements

The authors express appreciation to Richmond Mines Inc., for the easy access of drill cores and database of both Wasamac and Francoeur deposits. We also acknowledge the financial support of Richmond Mines Inc., of the Natural Sciences and Engineering Research Council (NSERC) and that of the Fonds Québécois de la Recherche sur la Nature et les Technologies (FQRNT) for this study which is part of an M.Sc. project by the first author (NM). In particular, we acknowledge Eric Marcoux, Stéphane Faure and Venetia Bodycomb for the review of the first version of the paper that truly improved the quality of this paper. The authors also address their acknowledgements to the reviewers Nicolas Thébaud and Bruno Lafrance for their careful reviews and insightful comments.

Appendix A

Sampling and analytical methods

Two sets of diamond drill core samples were selected for analysis: 28 samples for petrographic, geochemistry and LA-ICP-MS

studies, and another 16 taken at the scale of the shear zone for bulk rock geochemistry. The first set of 28 samples consists of altered units from the Main Zone, Zone 2 and Zone 3, along with their proximal unaltered host rocks for mass balance calculations. Samples dimensions ranged from 30 g to over 300 g each depending on the rock mass available: small sized samples are generally due to the very limited dimensions of typical altered samples of each alteration facies. The second set of 16 samples was collected by Richmond Mines Inc. during metallurgical testing. Macroscopic descriptions provided in the geological setting of the Wasamac deposit section of this paper were performed during drill core logging.

Polished thin sections of 22 samples from the first set were examined by optical microscopy, scanning-electron microscopy (SEM) using a Hitachi TM-3000 and laser-ablation inductively coupled mass spectrometry (LA-ICPMS). Laser ablation was performed with a M50 Resolution Excimer using a 193 nm UV beam. Vaporized matter was transported by He gas and ionised by plasma-Ar at 6000°K to a 7700x Agilent ICP-MS. Imaging was carried out by a series of parallel lines composed of successive 15 µm ablation spots. The following 26 elements were analyzed: Fe, S, Cu, Ti, Au, Ag, Te, Pb, Bi, Mo, Ni, Co, Zn, Hg, V, Pt, Cr, Mn, As, W, Ba, Sn, Sb, U, Se and Tl. Each ablation spot represents a pixel on the final mapping imagery for each element. The gold detection limit was fixed at 30 ppb. Details on instrument calibration are presented in [Allan et al. \(2005\)](#).

The whole rock geochemistry analytical methods for the 28 samples used fine crushing and powdering with carbon steel bowls to passing a 200 mesh (75 µm). An extra wash with glass has been conducted between each sample crushing. Four-acid digestion was then undertaken for the ICP-MS analyses and Li₂B₄O₇/LiBO₂ fusion for the XRF analyses. They were conducted by Acme Analytical Laboratories (Vancouver) Ltd of British Columbia, Canada. For the 16 samples, gold chemical composition was analyzed using a scanning-electron microscope equipped with an energy dispersive spectrometer (SEM-EDS). X-ray fluorescence (XRF), semi-quantitative X-ray diffraction (XRD) and ICP-MS analyses were also conducted on both FWSZ units and host rocks. These analyses were conducted by SGS Minerals Services of Lakefield, Ontario, Canada.

References

- Allan, M.M., Yardley, B.W., Forbes, L.J., Shmulovich, K.I., Banks, D.A., Shepherd, T.J., 2005. Validation of LA-ICP-MS fluid inclusion analysis with synthetic fluid inclusions. *Am. Mineral.* 90 (11–12), 1767–1775.
- Ayer, J., Amelin, Y., Corfu, F., Kamo, S., Ketchum, J., Kwok, K., Trowell, N., 2002. Evolution of the southern Abitibi greenstone belt based on U-Pb geochronology: Autochthonous volcanic construction followed by plutonism, regional deformation and sedimentation. *Precambrian Res.* 115 (1), 63–95.
- Ayer, J.A., Thurston, P.C., Bateman, R., Dubé, B., Gibson, H.L., Hamilton, M.A., Hathway, B., Hocker, S.M., Houlié, M.G., Hudak, G., Ispolatov, V.O., Lafrance, B., Leshner, C.M., MacDonald, P.J., Péloquin, A.S., Piercey, S.J., Reed, L.E., Thompson, P. H., 2005. Overview of results from the Greenstone Architecture Project: Discover Abitibi Initiative. Ontario Geological Survey; Open File Report 6154, p. 146.
- Beaudoin, G., Pitre, D., 2005. Stable isotope geochemistry of the Archean Val-d'Or (Canada) orogenic gold vein field. *Miner. Deposita* 40 (1), 59–75.
- Bédard, J.H., Harris, L.B., Thurston, P.C., 2013. The hunting of the snArc. *Precambrian Res.* 229, 20–48.
- Bigot, L., Jébrak, M., 2015. Gold mineralization at the syenite-hosted Beattie gold deposit, Duparquet, Neoproterozoic Abitibi Belt, Canada. *Econ. Geol.* 110 (2), 315–335.
- Blevin, P.L., 2004. Redox and compositional parameters for interpreting the granitoid Metallogeny of eastern Australia: implications for gold-rich ore systems. *Resour. Geol.* 54 (3), 241–252.
- Bonnemaison, M., Marcoux, E., 1990. Auriferous mineralization in some shear-zones: A three-stage model of metallogenesis. *Miner. Deposita* 25 (2), 96–104.
- Cabri, L.J., Chryssoulis, S.L., de Villiers, J.P., Laflamme, J.G., Buseck, P.R., 1989. The nature of “invisible” gold in arsenopyrite. *Can. Mineral.* 27 (3), 353–362.
- Cameron, E.M., Hattori, K., 1987. Archean gold mineralization and oxidized hydrothermal fluids. *Econ. Geol. Bull. Soc. Econ. Geol.* 82 (5), 1177–1191.

- Cassidy, K., Bennett, J.M., 1993. Gold mineralisation at the Lady Bountiful Mine, Western Australia: an example of a granitoid-hosted Archean lode gold deposit. *Miner. Deposita* 28 (6), 388–408.
- Ciobanu, C.L., Cook, N.J., Utsunomiya, S., Kogagawa, M., Green, L., Gilbert, S., Wade, B., 2012. Letter: Gold-telluride nanoparticles revealed in arsenic-free pyrite. *Am. Mineral.* 97 (8–9), 1515–1518.
- Colvine, A.C., Fyon, J.A., Heather, K.B., Marmont, S., Smith, P.M., Troop, D.G., 1988. Archean lode gold deposits in Ontario. Ontario Geological Survey, Vol. 139. Miscellaneous Paper, p. 136.
- Cook, N.J., Chryssoulis, S.L., 1990. Concentrations of invisible gold in the common sulfides. *Can. Miner.* 28 (1), 1–16.
- Cook, N.J., Ciobanu, C.L., Mao, J., 2009. Textural control on gold distribution in As-free pyrite from the Dongping, Huangtuliang and Hougou gold deposits, North China craton (Hebei Province, China). *Chem. Geol.* 264 (1), 101–121.
- Corfu, F., 1993. The evolution of the southern Abitibi greenstone belt in light of precise U-Pb geochronology. *Econ. Geol.* 88 (6), 1323–1340.
- Corfu, F., Jackson, S.L., Sutcliffe, R.H., 1991. U-Pb ages and tectonic significance of late alkali magmatism and non-marine sedimentation: Timiskaming Group, southern Abitibi belt, Ontario. *Can. J. Earth Sci.* 28 (4), 489–503.
- Couture, J.F., Pilote, P., 1993. The geology and alteration patterns of a disseminated, shear zone-hosted mesothermal gold deposit; the Francoeur 3 Deposit, Rouyn-Noranda, Quebec. *Econ. Geol.* 88 (6), 1664–1684.
- Cox, S.F., Wall, V.J., Etheridge, M.A., Potter, T.F., 1991. Deformational and metamorphic processes in the formation of mesothermal vein-hosted gold deposits – Examples from the Lachlan Fold Belt in central Victoria, Australia. *Ore Geol. Rev.* 6 (5), 391–423.
- Daigneault, R., Mueller, W.U., Chown, E.H., 2002. Oblique Archean subduction: accretion and exhumation of an oceanic arc during dextral transpression, Southern Volcanic Zone, Abitibi Subprovince Canada. *Precambrian Res.* 115 (1), 261–290.
- Daigneault, R., Mueller, W.U., Chown, E.H., 2004. Abitibi greenstone belt plate tectonics: the diachronous history of arc development, accretion and collision. *Developments in Precambrian Geology, The Precambrian Earth: Tempos and events*, Vol. 12, pp. 88–103.
- Dube, B., Gosselin, P., 2007. Greenstone-hosted quartz-carbonate vein deposits. *Mineral Deposits of Canada: A synthesis of major deposit-types, district metallogeny, the evolution of geological provinces, and exploration methods*. *Geol. Assoc. Can. Miner. Deposits Div. Spec. Publ.* 5, 49–73.
- Fleet, M.E., Chryssoulis, S.L., Davidson, R., Weisener, C.G., Maclean, P.J., 1993. Arsenian pyrite from gold deposits: Au and As distribution investigated by SIMS and EMP, and color staining and surface oxidation by XPS and LIMS. *Can. Miner.* 31 (1), 1–17.
- Gammons, C.H., Williams-Jones, A.E., 1995. The solubility of Au-Ag alloy + AgCl in HCl/NaCl solutions at 300°C: New data on the stability of Au (1) chloride complexes in hydrothermal fluids. *Geochim. Cosmochim. Acta* 59 (17), 3453–3468.
- Gao, J.F., Jackson, S.E., Dubé, B., Kontak, D.J., De Souza, S., 2015. Genesis of the Canadian Malartic, Côté Gold, and Musselwhite gold deposits: Insights from LA-ICP-MS element mapping of pyrite. In: Dubé, B., Mercier-Langevin, P. (Eds.), *Targeted Geoscience Initiative 4: Contributions to the Understanding of Precambrian Lode Gold Deposits and Implications for Exploration*. Geological Survey of Canada, Open File Report 7852, pp. 157–175.
- Genkin, A.D., Bortnikov, N.S., Cabri, L.J., Wagner, F.E., Stanley, C.J., Safonov, Y.G., McMahon, G., Friedl, J., Kersin, A.L., Gamyanyan, G.N., 1998. A multidisciplinary study of invisible gold in arsenopyrite from four mesothermal gold deposits in Siberia, Russian Federation. *Econ. Geol.* 93 (4), 463–487.
- Goldfarb, R.J., Baker, T., Dube, B., Groves, D.I., Hart, C.J., Gosselin, P., 2005. Distribution, character, and genesis of gold deposits in metamorphic terranes. In: *Economic Geology 100th Anniversary Volume*, Vol. 40, pp. 407–450.
- Goldfarb, R.J., Groves, D.I., 2015. Orogenic gold: common or evolving fluid and metal sources through time. *Lithos* 233, 2–26.
- Goldfarb, R.J., Groves, D.I., Gardoll, S., 2001. Orogenic gold and geologic time: a global synthesis. *Ore Geol. Rev.* 18 (1), 1–75.
- Goodwin, A.M., 1982. Archean volcanoes in southwestern Abitibi belt, Ontario and Quebec: form, composition, and development. *Can. J. Earth Sci.* 19 (6), 1140–1155.
- Grant, J.A., 1986. The isocon diagram; a simple solution to Gresens' equation for metasomatic alteration. *Econ. Geol.* 81 (8), 1976–1982.
- Groves, D.I., Goldfarb, R.J., Gebre-Mariam, M., Hagemann, S.G., Robert, F., 1998. Orogenic gold deposits: a proposed classification in the context of their crustal distribution and relationship to other gold deposit types. *Ore Geol. Rev.* 13 (1), 7–27.
- Groves, D.I., Goldfarb, R.J., Robert, F., Hart, C.J.R., 2003. Gold deposits in metamorphic belts: Overview of current understanding, outstanding problems, future research, and exploration significance. *Econ. Geol.* 98 (1), 1–29.
- Groves, D.I., Santosh, M., 2015. The giant Jiaodong gold province: the key to a unified model for orogenic gold deposits? *Geosci. Front.*, 1–9.
- Harris, L.B., Bédard, J.H., 2014. Crustal evolution and deformation in a non-plate-tectonic Archean Earth: Comparisons with Venus. In: *Evolution of Archean Crust and Early Life*, pp. 215–291.
- Hart, C.J., 2005. Classifying, distinguishing and exploring for intrusion-related gold systems. *Gangue* 87, 1–9.
- Hart, C.J.R., Goldfarb, R.J., 2005. Distinguishing intrusion-related from orogenic gold systems. In: *New Zealand Minerals Conference Proceedings*, pp. 125–133.
- Hart, C.J., Mair, J.L., Goldfarb, R.J., Groves, D.I., 2004. Source and redox controls on metallogenic variations in intrusion-related ore systems, Tombstone-Tungsten Belt, Yukon Territory, Canada. *Transactions of the Royal Society of Edinburgh. Earth Sciences*, Vol. 95 (1–2), pp. 339–356.
- Helt, K.M., Williams-Jones, A.E., Clark, J.R., Wing, B.A., Wares, R.P., 2014. Constraints on the genesis of the Archean oxidized, intrusion-related Canadian Malartic gold deposit, Quebec, Canada. *Econ. Geol.* 109 (3), 713–735.
- Hodgson, C.J., 1985. Notes for Short Course on Precambrian Lode Gold Deposits. Geological Association of Canada, Cordilleran Section, p. 70.
- Ispolatov, V., Lafrance, B., Dubé, B., Creaser, R., Hamilton, M., 2008. Geologic and structural setting of gold mineralization in the Kirkland Lake-Larder Lake gold belt, Ontario. *Econ. Geol.* 103 (6), 1309–1340.
- Jolly, W.T., 1978. Metamorphic History of the Archean Abitibi Belt. *Metamorphism in the Canadian Shield*. Geological Survey of Canada, Paper, pp. 10–78.
- Kerrich, R., 1983. Geochemistry of gold deposits in the Abitibi Greenstone Belt. *CIM Spec. Paper* 27, 75.
- Kishida, A., Kerrich, R., 1987. Hydrothermal alteration zoning and gold concentration at the Kerr-Addison Archean lode gold deposit, Kirkland Lake, Ontario. *Econ. Geol.* 82 (3), 649–690.
- Lang, J.R., Baker, T., 2001. Intrusion-related gold systems: the present level of understanding. *Miner. Deposita* 36 (6), 477–489.
- Lang, J.R., Baker, T., Hart, C.J.R., Mortensen, J.K., 2000. An exploration model for intrusion-related gold systems. *Soc. Econ. Geol. Newsl.* 40 (1), 6–15.
- Laporte, J., 2016. Mineralogical study of the auriferous shear zone along the Augmitto-Astoria segment in the Cadillac break south to Rouyn-Noranda, Abitibi, Quebec. Master thesis. Montréal (Québec, Canada). Université du Québec à Montréal, Maîtrise en sciences de la Terre, p. 243.
- Large, R.R., Danyushevsky, L., Hollit, C., Maslennikov, V., Meffre, S., Gilbert, S., Bull, S., Scott, R., Emsbo, P., Thomas, H., Singh, B., Foster, J., 2009. Gold and trace element zonation in pyrite using a laser imaging technique: implications for the timing of gold in orogenic and Carlin-style sediment-hosted deposits. *Econ. Geol.* 104 (5), 635–668.
- Large, R.R., Maslennikov, V.V., Robert, F., Danyushevsky, L.V., Chang, Z., 2007. Multistage sedimentary and metamorphic origin of pyrite and gold in the giant Sukhoi Log deposit, Lena gold province, Russia. *Econ. Geol.* 102 (7), 1233–1267.
- LeBas, M.J., LeMaitre, R.W., Streckeisen, A., Zanettin, B., 1986. A chemical classification of volcanic rocks based on the total alkali-silica diagram. *J. Petrol.* 27 (3), 745–750.
- Legault, M., Rabeau, O., 2007. Étude Métallogénique et Modélisation 3D de la Faille de Cadillac dans le secteur de Rouyn-Noranda (Phase 2). Ministère des Ressources Naturelles et de la Faune, Québec, p. 11. RP2007-03.
- MacLean, W., Barrett, T., 1993. Lithochemical techniques using immobile elements. *J. Geochem. Explor.* 48 (2), 109–133.
- MacLean, W., Kranidiotis, P., 1987. Immobile elements as monitors of mass transfer in hydrothermal alteration; Phelps Dodge massive sulfide deposit, Matagami, Quebec. *Econ. Geol.* 82 (4), 951–962.
- Mair, J.L., Farmer, G.L., Groves, D.I., Hart, C.J., Goldfarb, R.J., 2011. Petrogenesis of postcollisional magmatism at Scheelite Dome, Yukon, Canada: Evidence for a lithospheric mantle source for magmas associated with intrusion-related gold systems. *Econ. Geol.* 106 (3), 451–480.
- McCuaig, T.C., Kerrich, R., 1998. P-T-t deformation fluid characteristics of lode gold deposits: evidence from alteration systematics. *Ore Geol. Rev.* 12 (6), 381–453.
- McNicoll, V., Goutier, J., Dubé, B., Mercier-Langevin, P., Ross, P.S., Dion, C., Monecke, T., Legault, M., Percival, J., Gibson, H., 2014. U-Pb geochronology of the Blake river group, Abitibi Greenstone Belt, Quebec, and Implications for Base Metal Exploration. *Econ. Geol.* 109 (1), 27–59.
- Morey, A.A., Tomkins, A.G., Bierlein, F.P., Weinberg, R.F., Davidson, G.J., 2008. Bimodal distribution of gold in pyrite and arsenopyrite: Examples from the Archean Boorara and Bardoc shear systems, Yilgarn craton, Western Australia. *Econ. Geol.* 103 (3), 599–614.
- Mumin, A.H., Fleet, M.E., Chryssoulis, S., 1994. Gold mineralization in As-rich mesothermal gold ores of the Bogosu-Prestea mining district of the Ashanti Gold Belt, Ghana: Remobilization of “invisible” gold. *Miner. Deposita* 29 (6), 445–460.
- Neumayr, P., Walshe, J., Hagemann, S., Petersen, K., Roache, A., Frikken, P., Horn, L., Halley, S., 2008. Oxidized and reduced mineral assemblages in greenstone belt rocks of the St. Ives gold camp, Western Australia: vectors to high-grade ore bodies in Archean gold deposits? *Miner. Deposita* 43 (3), 363–371.
- Oliver, N.H.S., 1996. Review and classification of structural controls on fluid flow during regional metamorphism. *J. Metamorph. Geol.* 14 (4), 477–492.
- Perrault, G., Trudel, P., Bedard, P., 1984. Auriferous halos associated with the gold deposits at Lamaque mine, Quebec. *Econ. Geol.* 79 (2), 227–238.
- Phillips, G.N., Powell, R., 2015. A practical classification of gold deposits, with a theoretical basis. *Ore Geol. Rev.* 65, 568–573.
- Pilote, P., Couture, J.F., 1989. Gisements aurifères. Rouyn-Noranda. Ministère de l'Énergie et des Ressources du Québec, DV 89-05, pp. 95–96.
- Poulsen, K.H., Robert, F., Dubé, B., 2000. Geological classification of Canadian gold deposits. *Geol. Surv. Can. Bull.* 540, 106.
- Powell, W.G., Carmichael, D.M., Hodgson, C.J., 1995. Conditions and timing of metamorphism in the southern Abitibi greenstone belt, Quebec. *Can. J. Earth Sci.* 32 (6), 787–805.
- Putnis, A., 2002. Mineral replacement reactions; from macroscopic observations to microscopic mechanisms. *Mineral. Mag.* 66 (5), 689–708.
- Rabeau, O., Royer, J.J., Jébrak, M., Cheilletz, A., 2013. Log-uniform distribution of gold deposits along major Archean fault zones. *Miner. Deposita* 48 (7), 817–824.

- Rafini, S., 2014. Typologie des minéralisations aurifères associées à la Faille de Cadillac. Rapport du projet CONSOREM 2011-01 et 2012-01, p. 45.
- Robert, F., 1990. Structural setting and control of gold-quartz veins of the Val d'Or area, southeastern Abitibi subprovince. In: Ho, S.E., Robert, F., Groves, D.I. (Eds.), Gold and Base-Metal Mineralization in the Abitibi Subprovince, Canada, with Emphasis on the Quebec Segment, Vol. 24. University of Western Australia, Short Course Notes, pp. 167–210.
- Robert, F., 2001. Syenite-associated disseminated gold deposits in the Abitibi Greenstone Belt, Canada. *Miner. Deposita* 36 (6), 505–516.
- Robert, F., Brown, A.C., 1986a. Archean gold-bearing quartz veins at the Sigma Mine, Abitibi Greenstone belt, Quebec. Part I. Geologic relations and formation of the veins system. *Econ. Geol.* 81 (3), 578–592.
- Robert, F., Brown, A.C., 1986b. Archean gold-bearing quartz veins at the Sigma Mine, Abitibi Greenstone belt, Quebec. Part II. Vein paragenesis and hydrothermal alteration. *Econ. Geol.* 81 (3), 592–616.
- Sibson, R.H., Robert, F., Poulsen, K.H., 1988. High-angle reverse faults, fluid-pressure cycling, and mesothermal gold-quartz deposits. *Geology* 16 (6), 551–555.
- Sillitoe, R.H., 1979. Some thoughts on gold-rich porphyry copper deposits. *Miner. Deposita* 14 (2), 161–174.
- Sillitoe, R.H., 1991. Intrusion-related gold deposits. In: Foster, R.P. (Ed.), Gold Metallogeny and Exploration. Blackie, Glasgow, pp. 165–209.
- Sillitoe, R.H., 2002. Some metallogenic features of gold and copper deposits related to alkaline rocks and consequences for exploration. *Miner. Deposita* 37 (1), 4–13.
- Simard, M., Gaboury, D., Daigneault, R., Mercier-Langevin, P., 2013. Multistage gold mineralization at the Lapa mine, Abitibi Subprovince: insights into auriferous hydrothermal and metasomatic processes in the Cadillac-Larder Lake Fault Zone. *Miner. Deposita* 48 (7), 883–905.
- Smith, J.R., Spooner, E.T.C., Broughton, D.W., Ploeger, F.R., 1993. Archean Au-Ag-(W) Quartz Vein/Disseminated mineralisation within the Larder Lake – Cadillac Break, Kerr Addison – Chesterville System, North East Ontario, Canada, Ontario Geoscience Research Grant Program, Grant No. 364. Ontario Geological Survey, Open File Report 5831, p. 310.
- De Souza, S., Dubé, B., McNicoll, J., Dupuis, C., Mercier-Langevin, P., Creaser, R.A., Kjarsgaard, I.M., 2015. Geology, hydrothermal alteration, and genesis of the word-class Canadian Malartic stockwork-dissiminated Archean gold deposit, Abitibi, Quebec. In: Dubé, B., Mercier Langevin, P. (Eds.), Targeted Geoscience Initiative 4: Contributions to the understanding of Precambrian Lode Gold deposits and Implications for exploration, Vol. 7852. Geological Survey of Canada; Open File Report, pp. 113–126.
- Sutcliffe, R.H., Barrie, C.T., Burrows, D.R., Beakhouse, G.P., 1993. Plutonism in the southern Abitibi Subprovince; a tectonic and petrogenetic framework. *Econ. Geol.* 88 (6), 1359–1375.
- Thébaud, N., Rey, P.F., 2013. Archean gravity-driven tectonics on hot and flooded continents: controls on long-lived mineralised hydrothermal systems away from continental margins. *Precambrian Res.* 229, 93–104.
- Thompson, J.F.H., Sillitoe, R.H., Baker, T., Lang, J.R., Mortensen, J.K., 1999. Intrusion-related gold deposits associated with tungsten-tin provinces. *Miner. Deposita* 34 (4), 323–334.
- Trépanier, S., 2013. Norme Lithomodeleur. Rapport du projet CONSOREM 2011-04, p. 91.
- Witt, W.K., 1992. Porphyry intrusions and albitites in the Bardoc-Kalgoorlie area, Western Australia, and their role in Archean epigenetic gold mineralization. *Can. J. Earth Sci.* 29 (8), 1609–1622.
- Zhao, H.X., Frimmel, H.E., Jiang, S.Y., Dai, B.Z., 2011. LA-ICP-MS trace element analysis of pyrite from the Xiaqingling gold district, China: implications for ore genesis. *Ore Geol. Rev.* 43 (1), 142–153.
- Zhang, J., Lin, S., Linnen, R., Martin, R., 2014. Structural setting of the Young-Davidson syenite-hosted gold deposit in the Western Cadillac-Larder Lake Deformation Zone, Abitibi Greenstone Belt, Superior Province, Ontario. *Precambrian Res.* 248, 39–59.